UNIVERSITÁ DEGLI STUDI DI PAVIA

Facoltà di Ingegneria

Dipartimento di Ingegneria Civile e Architettura

TESI DI LAUREA

3D PRINTED REINFORCED CONCRETE BEAMS: STRUCTURAL RESPONSE AND ANALYSIS

Travi in calcestruzzo armato stampate in 3d: analisi del comportamento strutturale

Thesis of:

Stefano DELFRATE

Register n. 422063

Supervisor: **Prof. Ferdinando Auricchio**

Prof. Domenico Asprone

Co-supervisor : **Eng. Valentina Mercuri**

Eng. Costantino Menna

Academic year 2015-2016

A tutta la mia famiglia,

nella speranza che l'orgoglio di questo traguardo

possa ricompensare le loro fatiche

A mio nonno Ugo, appena scomparso,

che tu possa gioire di questo momento

con me, anche da lassù

Acknowledgements

Firstly, I would like to thank my supervisors, Prof. Ferdinando Auricchio and Prof. Domenico Asprone for the possibility to work and study with them the beautiful world of 3D printing.

Starting from the beginning, I would like to thank Gianluca Alaimo, for the introduction to Abaqus/CAE software and for his advices about it, and Marco Naclerio, for introducing me to the project and for his help during the first phase of the thesis. I would like to thank Costantino Menna, my first co-supervisor, for continuous directives provided during all phases of work.

Last but not least, a special thanks to my second co-supervisor, Valentina Mercuri, for her monumental patience with me. Without her help, I am sure, I would not be able to achieve this goal.

Abstract

Nowadays, in the fields of construction, civil engineering and architecture there is a growing demand for designing and building complex shapes using innovative materials and technologies. To meet this demand, engineers and researchers work in parallel to find the best solutions in terms of feasibility, speed of construction and costs.

In this framework, 3D printing technology is one of the most challenging solutions. Although it is still under development and not yet fully explored and exploited, the results obtained so far are very encouraging.

The aim of this document is to present an innovative technology for the 3D printing of reinforced concrete beams. The procedure consists in depositing fresh concrete layers one above the other thus creating monolithic blocks that are subsequently assembled in order to create complex shapes. Then, steel rebar reinforcement is externally installed only when the assembly is completed by anchoring the bars in specific holes produced during the printing process. Specifically, the object of the present study is the modeling and numerical analyses of the printed object to support the mechanical characterization of the same elements and to identify possible novel solutions. In this document considered geometries, materials and methods as well as the construction of the models and the setting of the analyses are reported in detail. Particularly, the focus is dedicated to the description of the boundary conditions, geometry configurations and loading conditions in order to draw conclusions and to understand the behavior of such elements when compared to traditional solutions.

Sommario

Al giorno d'oggi, nel campo dell'edilizia, dell'ingegneria civile e dell'architettura è sempre più in aumento la richiesta di progettare e costruire forme complesse utilizzando materiali e tecnologie innovative. Per soddisfare questa richiesta, progettisti e ricercatori lavorano in simbiosi per cercare le soluzioni ottimali in termini di fattibilità, velocità di costruzione e costi.

In questo contesto, la stampa 3D è una delle soluzioni che rispondono maggiormente a questa esigenza. Sebbene sia una tecnologia ancora in fase di sviluppo e ancora non del tutto esplorata e sfruttata a pieno, i risultati ottenuti finora sono molto incoraggianti.

L'obbiettivo di questo documento è quello di presentare una tecnologia innovativa per la stampa 3D di travi in calcestruzzo armato. La procedura consiste nel depositare strati di calcestruzzo fresco uno sopra l'altro creando così dei blocchi monolitici che vengono successivamente assemblati per creare forme complesse. In seguito, solo quando la fase di assemblaggio è completa, l'armatura è installata esternamente ancorando le barre nelle apposite cavità prodotte durante la fase di stampa. Nello specifico l'oggetto di questo studio è la fase di modellazione e di analisi numerica dell'oggetto stampato al fine di validarne la caratterizzazione meccanica e per identificare nuove possibili soluzioni. Saranno descritte in dettaglio le geometrie prese in esame, i materiali e le modalità di stampa e di assemblaggio delle componenti, nonché la costruzione dei modelli e l'impostazione delle analisi effettuate. In particolare l'attenzione sarà rivolta alla descrizione delle condizioni al contorno, delle configurazioni delle geometrie e delle condizioni di carico al fine di trarre delle conclusioni e di capire il comportamento dei suddetti elementi quando vengono confrontati con le soluzioni tradizionali.

Contents

List of figures

List of tables

1 Additive manufacturing

Additive Manufacturing is a process of incremental formation executed by the addition of subsequent layers of material without using supplementary instruments or molds, in a process that is fundamentally opposite to the milling subtractive procedure. The fundamental operation in the additive manufacturing process consists in slicing a solid model into sectional layers then converted through software in specific format, readable from the manufacturing machine. Between the many words used to define this technology, which is usually known as 3D-printing, the phrase “additive manufacturing” is the most suitable. It can be applied to various technologies not only the current ones, but also to future developments, for example multi-axial applications. Shapeless materials such as liquids, powders, gas and fibers are turned into uniform solids by physical and chemical processes. One of the best advantages of this process is to create unique components, which couldn’t be feasible or could be very expensive if traditional production techniques were used. Moreover additive manufacturing offers an high degree of freedom to design shape. Another key point of this kind of processes is at economical level: there are great advantages in particular the lowering of production costs because many natural or recyclable materials are used. These characteristics lead to a greater involvement of architects and designers in this field to meet the increasing need of customization of structure by customers [1].

1.1 Evolving of 3D Printing

The first process of additive manufacturing was conceived by Chuck Hull (1986) who invented the process called Stereolithography (SL), which consist of solidification of subtle layers of ultraviolet ray-sensitive liquid by a computer controlled laser. Moreover, Hull designed a kind of file called STL (Standard Triangulation Language). It is currently used in digital slicing and buffering processes which are widespread in many 3D-printing techniques. From this period on, in the field of additive manufacturing there has been an exponential growth thank to the development of many production methods.

Some prototyping technology in alternation to stereolithography have been used since 1991, such as Fused Deposition Modeling (FDM), the first printing technology. It was the laying down of layers of thermoplastic material extruded with threads, which was sold by Stratasys. In the following years other additive manufacturing technologies were put into market:

- SGC (Solid Ground Curing): that used a UV-sensitive liquid polymer solidifying full layers in one pass by flooding UV light through masks created with electrostatic toner on a glass plate;
- LOM (Laminated Object Manufacturing): that bonded and cut sheet material using a digitally guided laser;
- SLS (Selective Laser Sintering)

Nowadays, there are about fifty additive manufacturing procedures which are based on many chemical and functional principles, which are used in each stage of production and design processes of the components and which guarantee a few limitations concerning shaping, complexity and composition of material. The demand of additive processes in the field of building is more and more increasing, in particular for the development of technology able to increase the speediness of constructing and which are mainly based on the study of new natural materials which are suitable at physical and chemical level to construction demand in the field [1].

1.2 3D printing in Architecture and Construction

Construction activity can be conceived as an additive process where many sub-components are laid down. Additive manufacturing can be applied in the field of AEC (Architecture, Engineering and Construction) sector essentially in two ways:

- to produce components and sub-components to be assembled and joined in order to create larger structures;
- to print large-scale and self-standing architectural elements as a whole.

Large-scale 3D printing has some useful advantages:

1. to allow to build complex geometries without the elevated cost of manual labor;

2. to remove temporary structures;
3. to reduce the time of construction;
4. to allow unseen levels of freedom in the design and realization of forms.

Many researchers teams and companies have tried to applied the manufacturing technology to construction field since the first half of the nineties, but today it is still a challenge for them. The greatest problem in this field concerns the size of printing machine available in comparison to the size of buildings which are to be printed. To resolve this problem many studies are made recently, to develop large-scale 3D-printers and at the same time to test new materials suitable to the technology applicable to construction field [1].

1.3 Large-Scale 3D Printing

1.3.1 Contour Crafting

The first attempts to build a full 3D-printed building were made in USA though a Contour Crafting technology, and in Italy though a D-Shape technology. With the latter, the automatized production technology is applied for the first time to construction field. The Contour Crafting allows the great reduction in the placing of the components and to cut down the costs (75% estimated)

This technology is a combined process, indeed it use both the extrusion, which creates the profile of the thing and the injection, which creates the inner part of the thing. The nozzle has two plates, a frontal one and a side one, which promote the smooth surfaces realization in each layer; the side plate can be bent to make no-orthogonal surfaces. A great advantage of this technology is to place thicker material layers in comparison to other methodologies, such as those using sticky liquids, thank to the two plates above mentioned. This advantage allows the great reduction of production charges, a main characteristic for the applications of large-scale additive manufacturing.

The wide range of materials used allows the better choice according to the own's needs. The drying times of the material are quick, guaranteeing the support of the following layers allowing the self-sustaining of the printed structure [1].

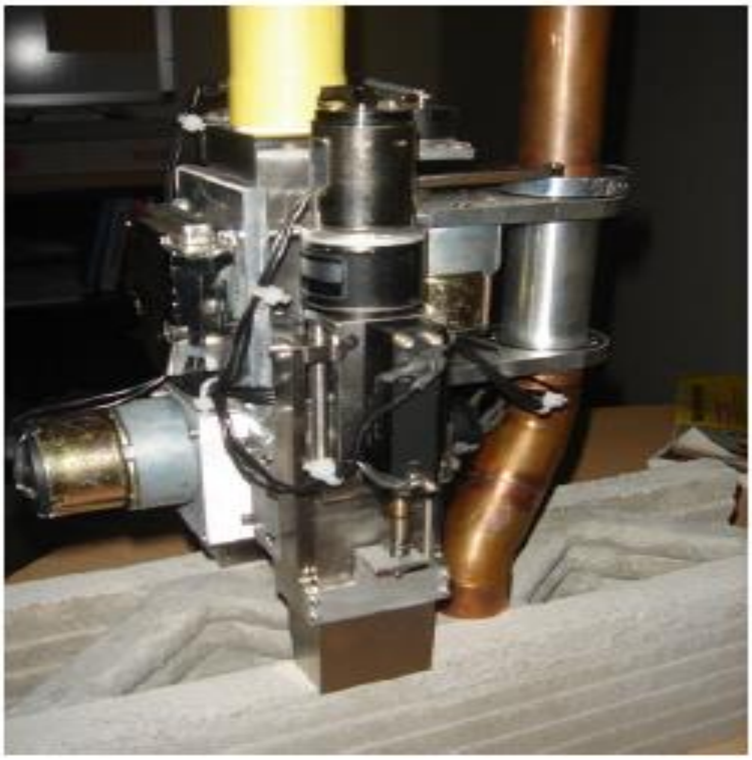

Figure 1.1 Contour Crafting printing process, taken from [1].

1.3.2 D-Shape

The Italian engineer Enrico Dini developed D-Shape technology in 2004. This 3D-printing system is similar to the others ones, it concerns the injection of sand and epoxy resin which are mixed together and laid down with layers which are 5-10 mm thick. The actual printable area is 6 by 6 m and theoretically unlimited high, defined anyway by the self-sustaining capacity of the structure. The data concerning geometry deriving project design are verified by a finite element software and if it is the case, optimized. After this phase the data were converted into the STL language and transferred to the printing machine, with the beginning of the real printing process.

The sand is laid down in layers and a following spray adds the liquid, which causes a catalytic reaction infiltrating into the grains. In this way, powder is turned again into the rock from which it derived, looking like marble [1].

Figure 1.2 D-Shape, taken from [1]

1.3.3 Emergency 3D printing of houses

The contour crafting and the D-Shape were the first experiments of application of 3D-printing in the field of construction but they were not the only applications that were developed. In 2014, the Chinese company WinSun decoration Design Engineering Co. used an enormous printer which was 150 by 10 by 6 m to print ten houses in less than twenty-four hours. The houses (195 m^2) were built with a budget of less than 5000 dollars, showing that the technological equipment and technical skills can be available by a few years, with a cheaper and faster alternative in case of emergency or for the social lower classes [1].

1.4 Manufacturing Building Components

1.4.1 Materials

The additive manufacturing technology uses mainly the granular materials making waste material very cheap to be used. The research project Emerging Object is aimed at apply the uncommon materials to 3D-printing techniques also including SLS, FDM, and LOM. Some of the tested solutions are:

- polymers
- wood
- paper
- chocolate
- salt

the result of this research is the realization of 3D-printed house 1.0, commissioned by Jin Hai Lake Resort Beijing. It was developed combining the traditional technologies and 3D-printing ones.

The fundamental idea is based on a spaces differentiation. Small-scale printing machines were used to create various components using different material, such as salt and glue, which are assembled together at a later time [1].

Figure 1.3 An example of 3D printed wood as a possible building material obtained by waste, taken from [1]

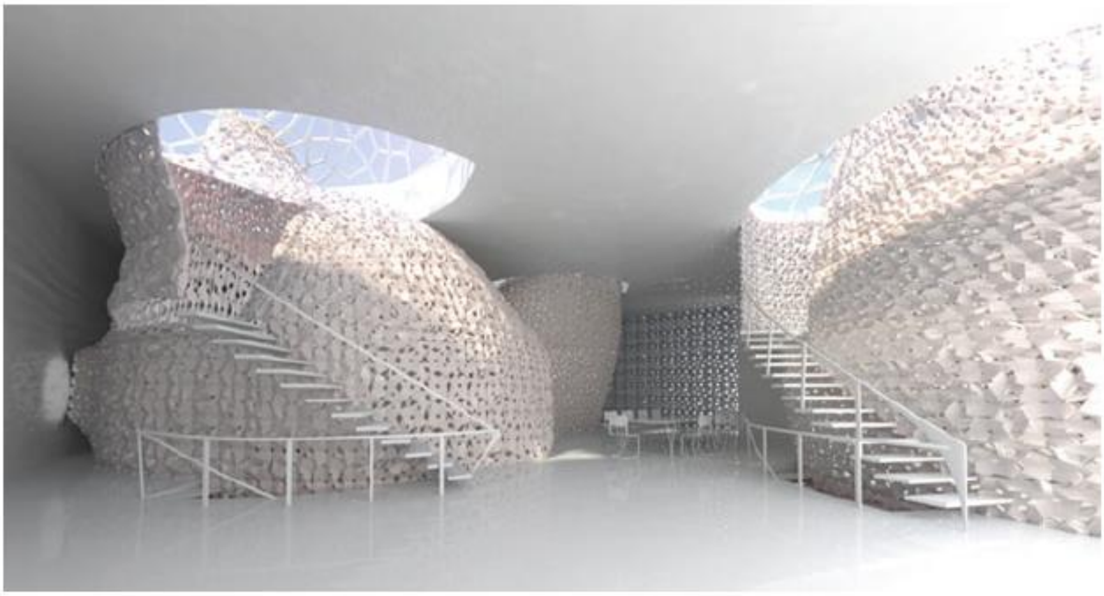

Figure 1.4 3D printed house 1.0, interior space, taken from [1]

Figure 1.5 Recycle paper employed for 3D printing a house, taken from [1]

1.4.2 3D Printed Steel Joints

A research team lead by Arup developed a 3D-printing technique of steel joints during a project in collaboration with WithinLab, CRDM/3D Systems and Eos. Arup's idea was to give a solution for the joints of lightweight tensile structure characterized by a complex shape and very customized design. The process developed by researchers is based on additive laser sintering principle and employs steel derivatives as printing materials.

The original material of the structure nodes was stainless steel and then marging steel, a far stronger material than normal construction steel. The DMLS (Direct Metal Laser Sintering) advantages are:

- weight reduction;
- geometrical freedom preservation
- waste materials minimization

Larger machines and hybrid materials were used to meet the specific demands of customers and designers [1].

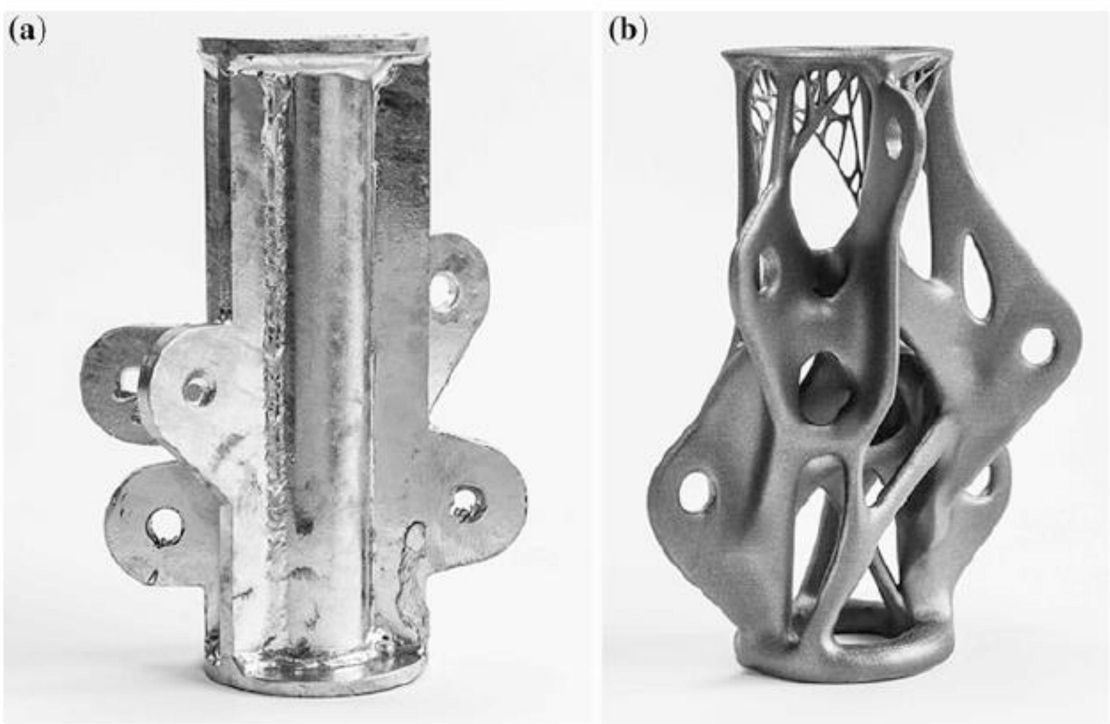

Figure 1.6 a) steel joint produced with traditional techniques; b) 3D Printed Steel Joint , taken from[1].

1.4.3 Robotic printing

In the field of buildings, the size problem related to the dimensions of printing machine is partially resolved thank a researchers team of the Institute for Advanced Architecture of Catalonia (IAAC). They elaborated a manufacturing system using robots called Minibuilders able to 3D-print. They are divided in three categories with complementary functions:

- Foundation robots: are employed at the beginning for the printing of the first twenty layers. They are sustained through pipes and are linked to auxiliary robots providing printing material;

- Grip robots: they grip themselves to the newly printed structure and help the placement of the following layers. Each layer is dried immediately printing to allow the fix of the same robots to the following step. Because of the great fixing force this kind of robots also allows the realization of ceilings and curved walls.
- Vacuum robots: they are used to reinforce the newly printed structure. They move up and down on construction and place additional layers of material in the necessary points, on a perpendicular plane in comparison to the other layers.

Although this technology must be improved, it is a reliable instrument to overcome the size limits of 3D printers and to allow the realization of whole buildings [1].

Figure 1.7 The Grip Robots cramp themselves to the existing structure, and thanks to their four rollers, they create curved walls, taken from [1].

1.4.4 3D Concrete Printing

The Innovative Manufacturing and Construction Research Centre (IMCRC) at the Loughborough University started the Freeform Construction project, in collaboration with the UK Engineering and Physical Science Research Council (EPSRC) and other partners. The printing machine developed by the researcher is characterized by a printing area of 2 by 2 by 2 m and it is based on a principle similar to the Fused Deposition Modelling (FDM). The difference concerns, in this case, the placement of the concrete by a nozzle, working at constant speediness. What differentiates this technique from the aforementioned Contour Crafting and D-Shape is the possibility of printing large-scale volumetric components on-site. Some of the most meaningful advantages of this technology are:

- achievement of structurally optimized constructions;
- functional integration;
- the reduction in the assembly complexity [1].

Figure 1.8 Free-form construction, this figure shows a complex geometry allows by this technology, taken from [1].

1.4.5 Anti-gravity 3D Printing

Conventional methods of additive manufacturing have been typically restricted by gravity and printing techniques based on 2D layers that ignore the object structure. Another way to neutralize the gravity effect during the course of the printing process is an intelligence choice of the material, combined with the use of innovative extrusion technology that allows the creation of 3D curves. A new method was developed by IAAC and Joris Laarman Studio: it allows to produce objects with three-dimensional curves, irregular height buildings, inclined curves and vertical surface. The design team worked on the production of the prototype of the extruder and at the same time numerous material experimentation had been done to create an appropriate material and its mixture. In the initial phase, acrylic tubes were used as extruder cask attached to the robotic arms, but the high viscosity of the material imposes the use of aluminum ones.

After several attempts, a 50 cm long spiral line connected to a vertical surface was printed.

The two fundamentally problems were:

1. combination and synchronization of the robotics movements;
2. material extrusion.

The sustaining elements can be avoided, thanks to the combination of a new extrusion technology and the hardening thermos-resin [1]

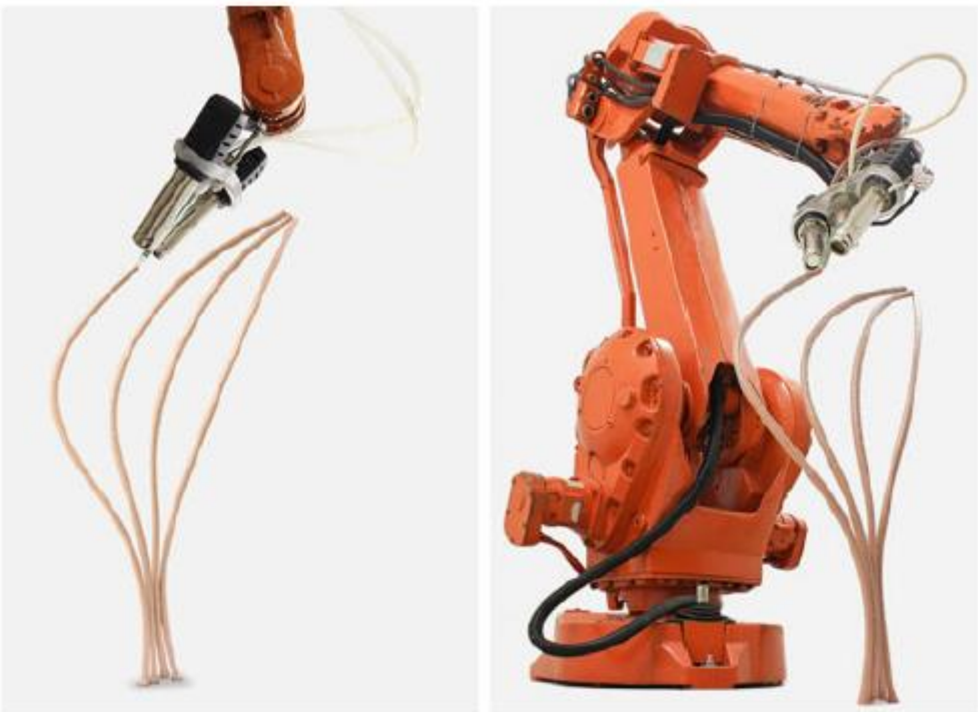

Figure 1.9 Anti-gravity 3D printing, with the help of the robot and the new extrusion technology the gravity effect is neutralized, taken from [1].

1.5 Thesis aims and organization

3D printing technology presents a range of uses in many different sectors of production, science and research. In particular, within the field of architecture and civil engineering, we try to employ this technology to optimize the sections in terms of shape, weight and functionality.

The idea of studying the behavior and the creation of reinforced concrete beams, comes from the collaboration between the University of Naples Federico II and the University of Pavia, involving the respective research departments.

The basic idea is to divide the object of study in several segments which are then printed separately and subsequently assembled with the external reinforcement bars. Before the printing phase, the beam is modeled with a finite element software (Abaqus / CAE) to predict the behavior of the printed objects and to study the optimization.

The aim of this thesis is to conduct numerical analyses, considering both linear and non-linear problems. Particularly, for the material modelling, in a first step we define a perfectly elastic material and in a second step an elastic-plastic one. Furthermore, different boundary conditions and load configurations are considered, in order to obtain accurate results.

The document is structured as follows:

- **Chapter 2:** this chapter introduces a general description of the technology. Some preliminaries on structural, topological and shape optimization are also reported;
- **Chapter 3:** this section provides an overview of the case studies, the geometries, the configuration of the section thickness and analysis types. It also introduces the constitutive model used for the non-linear analyses and the results of the tensile tests carried out on a sample to show the characteristic behavior of the material:
- **Chapter 4:** it describes in detail all the analyses, the boundary conditions and load combinations considered together with the construction of the model. It

also shows the results obtained from the analyses along with some graphics and representative plots of the structural performance response;

- **Chapter 5:** conclusions about the results and future developments.

2 Novel approach for the manufacturing of complex shape

The use of 3D printing makes possible the production of extremely complex structures, which up to a short time ago, using the traditional production methods, would have been impossible to achieve or would have required unsustainable efforts and unthinkable costs. Before describing the method developed for the printing of reinforced concrete elements, optimization and structural optimization concepts are explained. Optimization is, indeed, a fundamental step in the additive manufacturing process because it allows to increase printing speediness and, at the same time, to reduce printing time of things and to save material, and as a consequence to drop the costs.

2.1 Concepts of optimization and structural optimization

The field of optimization is a branch of applied mathematics which studies the theory and research methods of the extremes in a model which transforms a given physical problem in mathematics terms. It is the mathematics instrument which allows us to find the best solution for a problem, where the aim is attained though the definition of the combination of the factor influencing the same problem. The optimization variables are modified with iterative techniques in each step of the process to find the best solution possible[2].

According J. E. Gordon's words, a structure is defined in mechanics as "any assemblage of materials which is intended to sustain loads" [3]. Structural optimization is aimed therefore at guaranteeing this function in the best way possible. It is necessary to specify the phrase "best" in this case: best is referred to the fact that structural optimization makes structure very light and reduce weight, preserving the maximal stiffness to avoid global or local instability. An optimization process can't be, obviously, started without any suited constraints, otherwise the solution would not be well defined. Among the constraints which usually used we can mention stresses, displacements and/or geometry [3][4]. The optimization process can be summarized in three elements:

- decision variables: are the variables whose optimal values are to be defined;

- target function: is the variable which is to be minimized or maximized;
- acceptable set: is the set which contains the possible solutions.

Following, the three main categories of optimization are reported:

- Parametric optimization
- Topology optimization
- Shape optimization

2.1.1 Parametric optimization

In this kind of optimization, some parameters of the calculation model, are defined firstly by the user. A validity range between a minimum and maximum is typically assigned to the parameters, on which the optimization software can work to reach the goal. Classic examples of optimization parameters are the thickness of the plate (in FEM models to shell elements), the elastic modulus of the material and the connecting elements stiffness. A particular case of parametric optimization is the discrete variables optimization, in which the optimal solution is not sought for any values of the parameters but only between predefined ones [5].

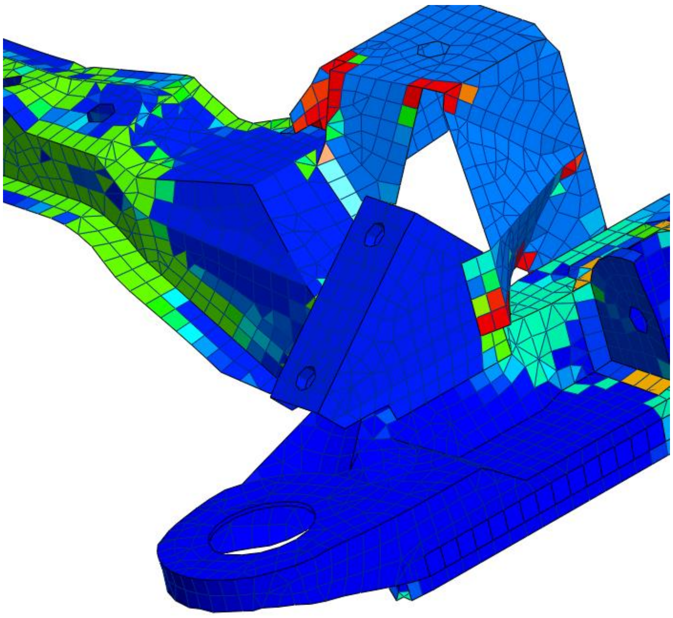

Figure 2.1 Example of parametric optimization taken from [5]

2.1.2 *Topology optimization*

An automatic optimization algorithm is able to indicate to the designer the optimal shape of a component for a set of prescribed constraints. The main difficulties in a topology optimization procedure is to obtain feasible geometries, especially if the component production technology is already fixed.

In this sense it is possible to insert some information in the optimization, related to the constructive aspects, such as the extrusion direction in the case of an extruded component [5].

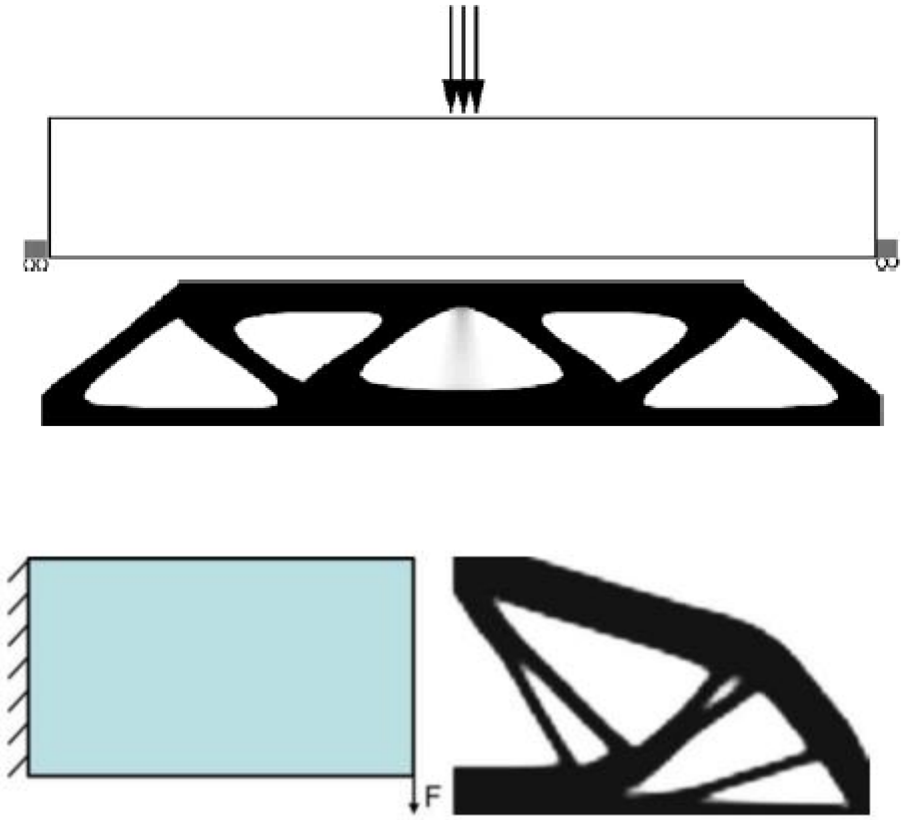

Figure 2.2 Examples of topology optimization, taken from [4] and [7]

2.1.3 *Shape optimization*

Shape optimization is a process where the geometry of a things is modified to perform a task in the best way possible. Using the finite element method, starting from a first attempt model, new shapes are created using the same number of nodes and elements, preserving the same starting topology.

In this case, a Mesh Morphing techniques are used to modify, globally or locally, the mesh of the analytical model in order to improve the desired performance in terms of overall stiffness or local resistance. This technique requires the implementation of a reference calculation model, which is named “baseline design” that will be made parametric through the Morphing application. Once defined the geometric changes and their variance field, they can be applied simultaneously to the baseline design, in order to determine a modified design which evaluate the performances [5].

Typically this technique is combined with the optimization approach called Design-of-Experiments (DoE), with which a limited numbers of modified models is generate. Through the response of the modified models (experiments) a response surface is calculate, that is a function of the geometric variables of the project, through which the optimal design is determined.

In the following picture is reported a simple example of shape optimization. If we hold the sheet horizontally, it is not able to sustain the self-weight and any other object but if we bend it slightly instead, it can sustain both [6].

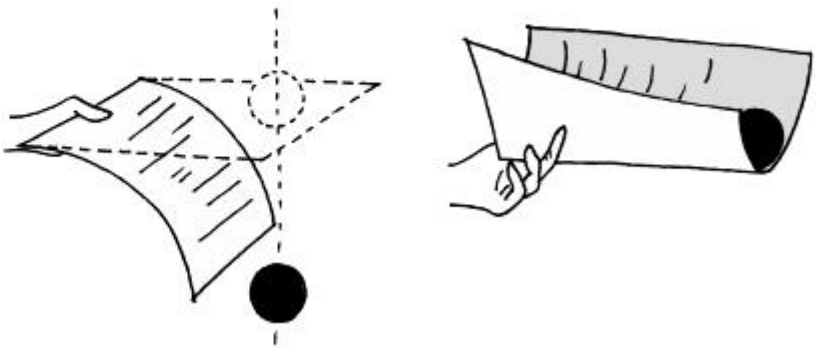

Figure 2.3 Example of shape optimization taken from [6]

Optimization is an important aspect for 3D-printing, in particular our focus is the topology optimization, where target function is mass and the constraints which must be followed concern the stresses and the displacements. However, in this document, these details cannot be analyzed because these mentioned principles are not applied to the current beams, but these will be applied for the construction of further beams in future projects.

2.2 Consideration about the optimization and the proposed printing method

In this case a more traditional approach used as the application of 3D-printing technology is in an experimental phase in the field of civil engineering. The approach used is based on the Ritter-Mörch spatial trellis, which allows to detect the trend of internal stresses in the concrete and as a consequences the zone where we can remove material to lighten the section without changing the resistance and stiffness features of the beam. The current studies aim at introduce these optimization algorithms, which are, without any doubt, reliable and fast instrument device to obtain the expected result.

3 Test cases

This chapter provided an overview on the two analyzed geometries. It also describes the two configurations of thickness and which types of analysis (linear or non-linear) have been performed. It will be introduced in this section the constitutive behavior used for non-linear analyses and are also presented graphs taken from simulations carried out with Abaqus to test its effectiveness.

3.1 Geometries

Before going into details in the description of the characteristics of each beams and the analysis methodology, we need to specify that the two beams examined were already printed and assembled by the Department of Structures for Engineering and Architecture of the University Federico II of Naples. While the assembly and print phases were carried out in Naples, the design, model, and analysis phases are carried out in collaboration with the Department of Civil Engineering and Architecture of University of Pavia.

The linear analyses have been performed before printing, to study the trend of the stresses in a representative model of a classical beam with the compact section to analyze the performance of the internal stresses. By studying the latter it has been proposed a modeling approach based on the strut and tie approach in order to lighten the beam by the self-weight trying to maintain the strength characteristics.

3.1.1 Straight beam

The first beam that has been the object of this project is 3.5 m long with a rectangular section with a width of 0.2 m and a height of 0.4 m. The beam was divided into seven segments of two types:

- ✓ Type A: this section characterizes six of the seven segments that make up the entire beam, having a shape that resembles a "S" and placed in a symmetrical way, three on each side next to the central block;
- ✓ Type B: the only element of this type is the central block which has the shape that resembles a "T" that has the keystone function in the beam.

In the Figure 3.1 the subdivision into segments and the geometries of the two elementary blocks are represented.

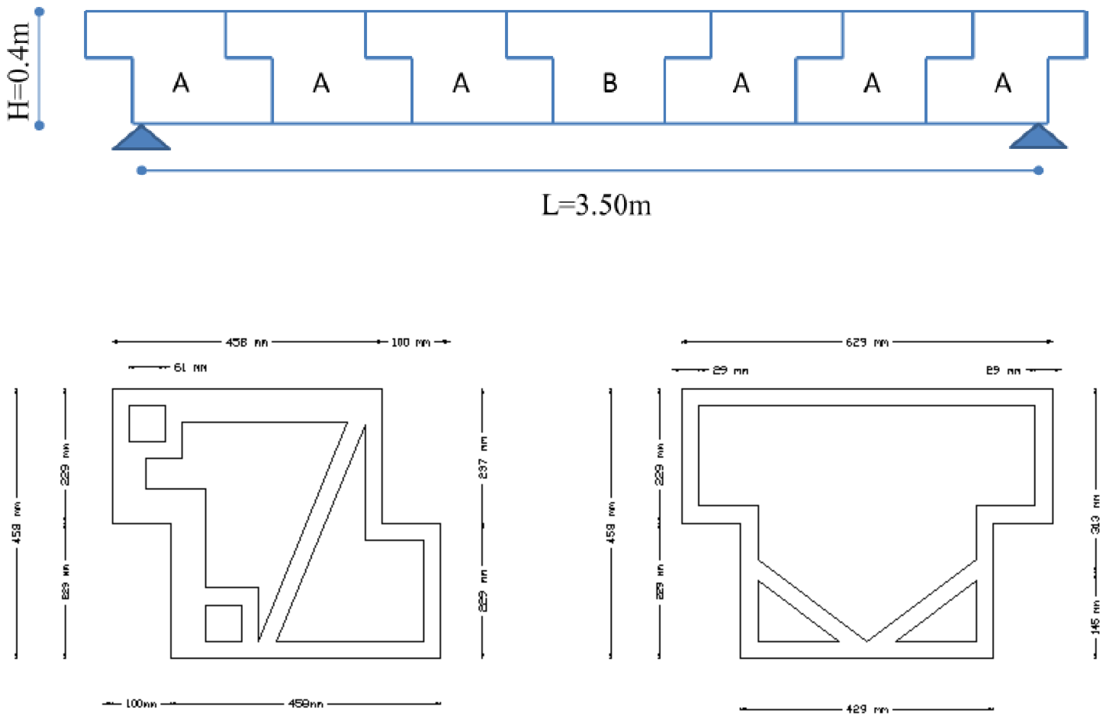

Figure 3.1 Beam division and elementary blocks

The first step is to create a CAD model (Computer Aided Design) subsequently imported in the Abaqus/CAE Finite Element software for constructing the complete numerical model and then estimating the deflection and the deformability of the beam.

The concrete parts have been modelled with eight-nodes elements while the steel bars with a truss element and an elastic constitutive behavior was adopted for both materials.

The following figures show the CAD model with the rebar system. As we can see from the figure, the rebar system is composed by three type of bars with different characteristics:

- Type 1: diameter equal to 8 mm and length equal to 770 mm;
- Type 2: diameter equal to 10 mm and length equal 560 mm;
- Type 3: diameter equal to 10 mm and length equal 830 mm.

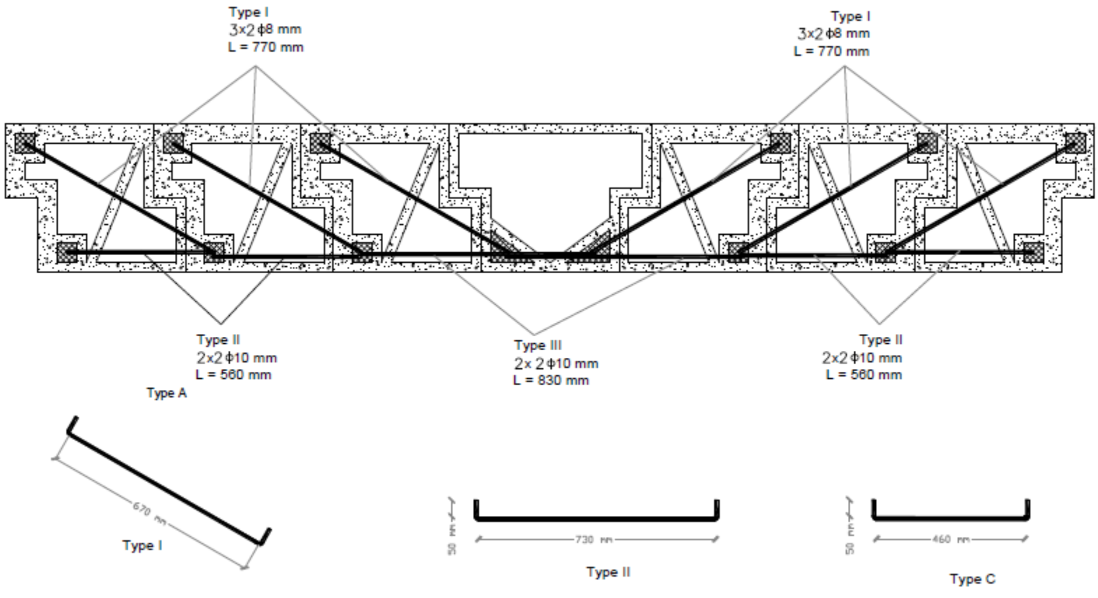

Figure 3.2 Cad model

3.1.2 Curved beam

The second 3D printed beam is an irregular arc, about 4.0 m long with a width equal to 0.25 m.

Such irregular form has been chosen to exploit the basic additive manufacturing idea, i.e., that 3D printing allows to realize freeform sections and elements respect to traditional manufacturing techniques. The initial beam design is depicted in the figure below:

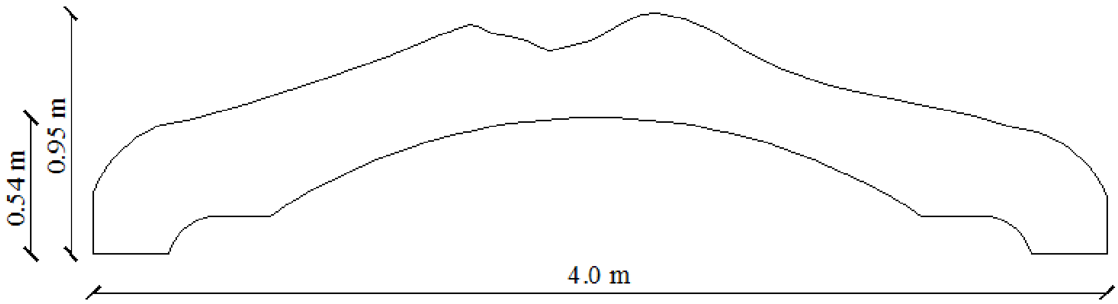

Figure 3.3 Initial design

The process is the same adopted for the first beam, a CAD model has been imported in the Abaqus/CAE software and the numerical model has been created to investigate the approximately behavior of the beam in terms of deflection and stresses.

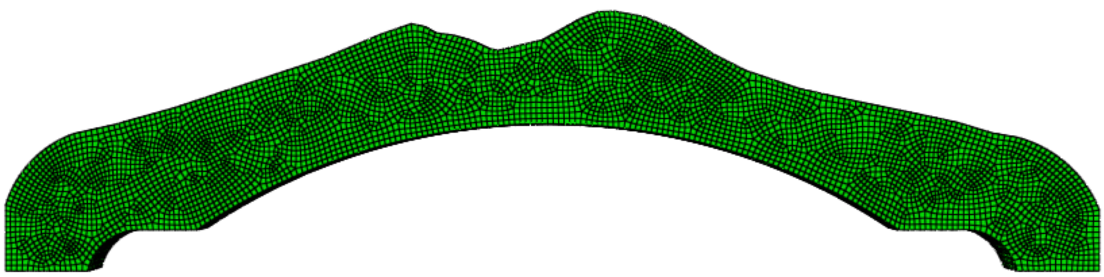

Figure 3.4 Mesh of the initial configuration of the second beam test

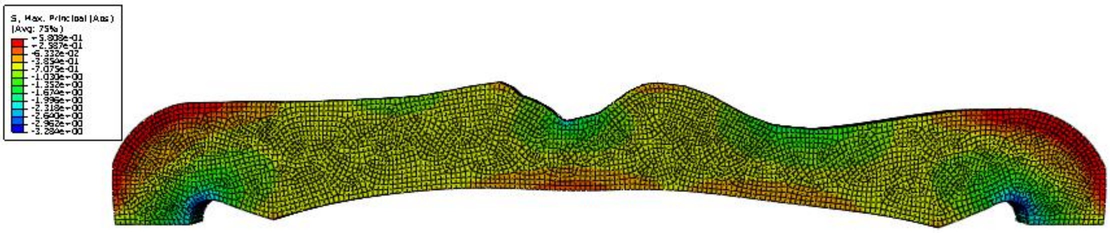

Figure 3.5 Deformed configuration of the beam and stress plot

It must be specified that only some results about straight beam will be reported because the whole work had already finished before the beginning of this project. Concerning the curved beam, the main topic of this document and on which the author worked about, both the step of numerical analysis and project step from the preliminary test will be reported.

3.1.2.1 Preliminary tests on the curved beam

Starting from this simple analysis, three different configuration based on the Ritter-Mörsch strut and tie trellis model have been created.

The beam has been divided into ten parts which are all different one from each other; a post-rebar system has been applied during the assembly phase.

Subsequently, three cases of preliminary tests have been implemented, based on the same configurations described, for estimating the deflection and the stresses.

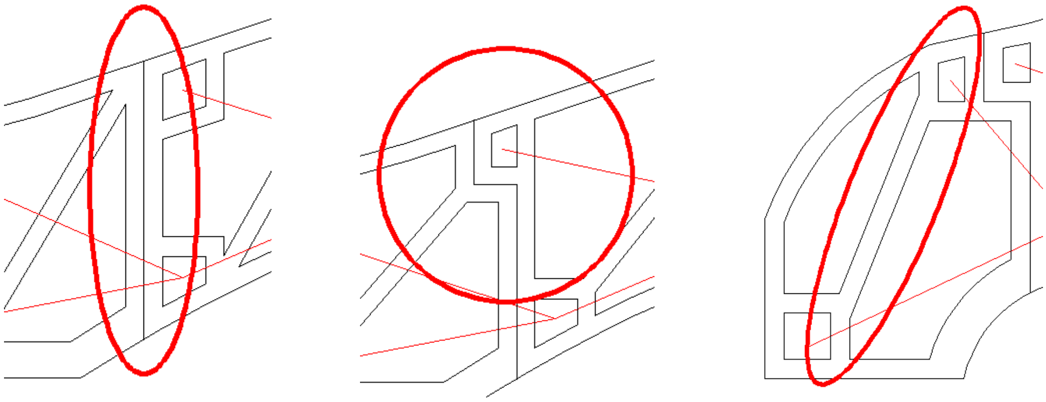

Figure 3.6 Difference between the three configurations

1. Configuration 1: ten elements with vertical lateral sides

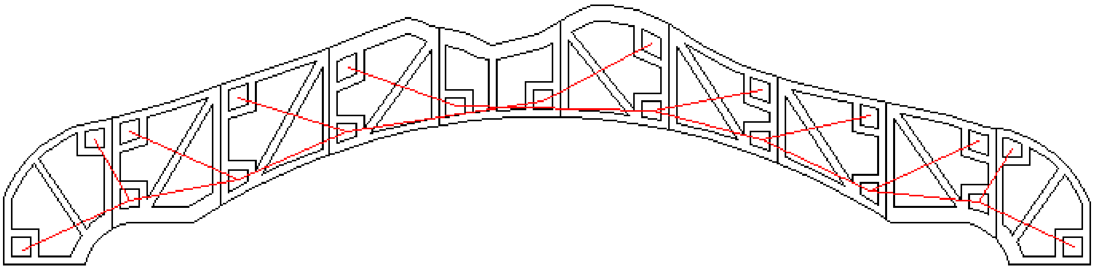

Figure 3.7 Configuration 1

2. Configuration 2: ten elements with step-form lateral sides

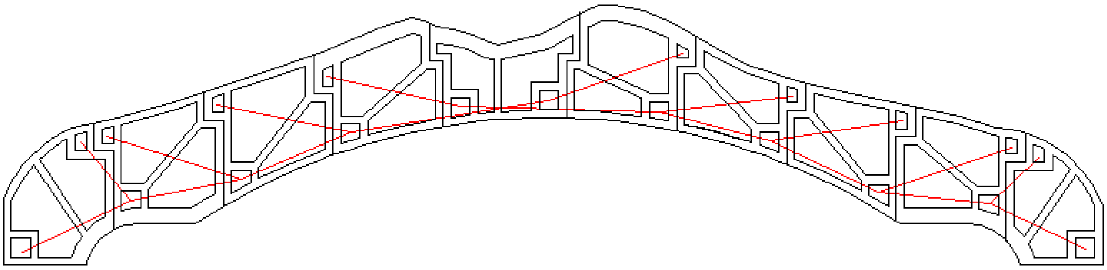

Figure 3.8 Configuration 2

3. Configuration 3: the only difference with configuration 2 is that in the extremity elements the strut inclination change

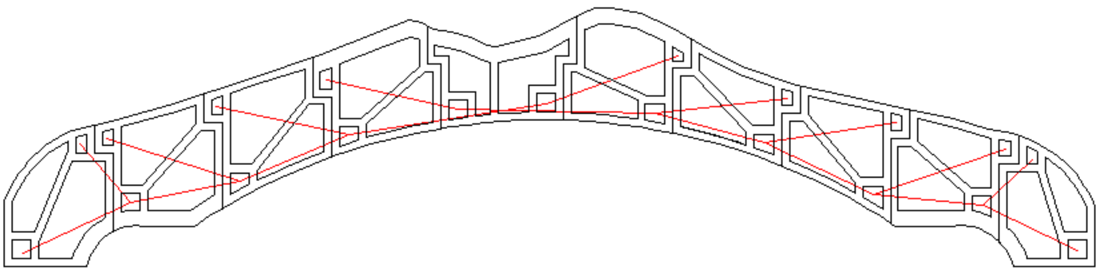

Figure 3.9 Configuration 3

3.1.2.2 *Final geometry configuration*

After the preliminary analyses, the model has been improved restarting from the cad configuration. The final configuration is approximately the same with some improvements like as the repositioning of the bars hole, the outline thickness configuration, the vertical side of the singular elements and the rebar system configuration.

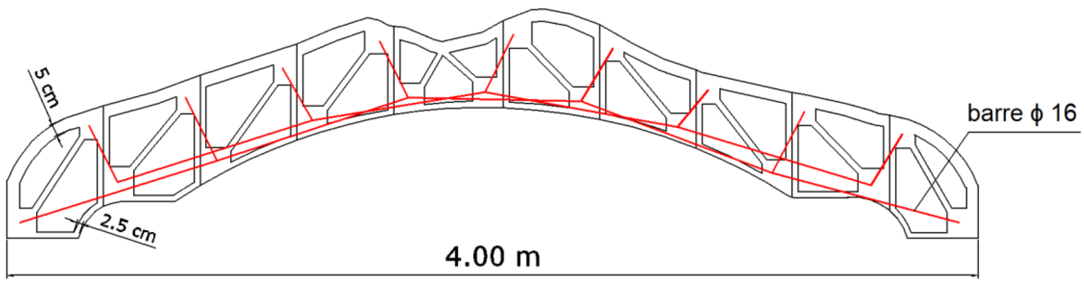

Figure 3.10 The new beam configuration

3.2 Thickness configurations

In this subsection the thickness configurations adopted for the analyses will be described. The edge thickness of each block is related to the nozzle that sprays the fresh concrete. For the first printed beam, the nozzle had a diameter equal to 25 mm then the thickness of the outline of the block had the same size if there was a single path line, and 50 mm if there was a double path line.

For the second beam, instead, two thickness configurations have been supposed:

1. Thickness 1: only the top side of the beam has a double path line with a thickness of 50 mm, while the rest of the model has a 25 mm of thickness;
2. Thickness 2: the whole model has a double path line with the exception of bar hole cords.

The nozzle for these two configuration has been expressly 3D-printed for this purpose by the department of Civil Engineering and Architecture, University of Pavia.

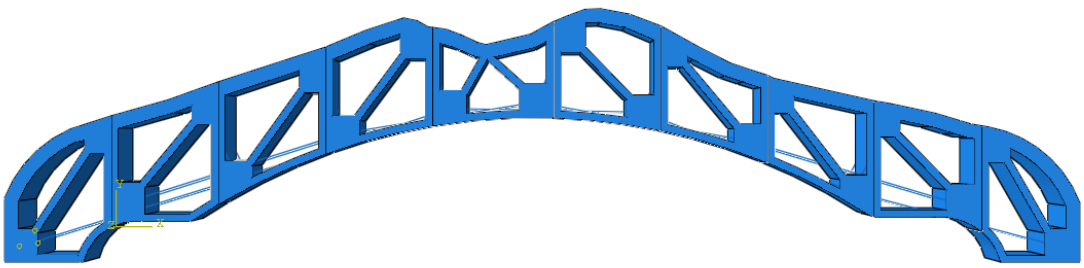

Figure 3.11 Thickness 1

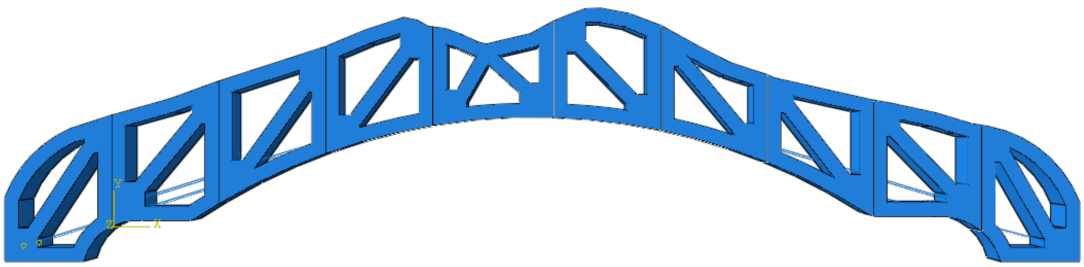

Figure 3.12 Thickness 2

3.3 Analyses description

In this subsection the kinds of analyses carried out will be described, focusing our attention on the controlled displacement analyses and explaining the meaning of:

- linear analyses
- non-linear analyses

With the first ones we mean that in the material property has been employed an elastic constitutive behavior for both materials, steel and concrete. This approach has been utilized for the analyses on the first printed beam and on the linear analyses (mentioned in the paragraph 3.1.2.2) about the curved beam.

The material parameters employed in the linear analyses on the first and on the second beam are reported in the table below:

	Concrete	**Steel**
E (Gpa)	30	210
ν	0,2	0,3

Table 3.1 Materials parameters for the straight beam

	Steel	**Concrete**
E [MPa]	210	30
ν	0.3	0.2
P [Ton/mm3]	7.8E-09	2.24E-09

Table 3.2 Materials parameters for curved beam

In the second group of analyses, instead, it has been implemented an elastic-plastic constitutive behavior described in the next paragraph.

On curved beam, for both typologies described over there, the two thickness configuration have been used and combined with two constraints employed: contact and tie.

The non-linear analyses have been conducted in the following ways:

- the first group of analyses encompasses the four base model analyzed in which only the concrete parameters have been changed. These analyses have been implemented to obtain a direct comparison with the linear ones in terms of order of magnitude of the results;
- the second and larger group encompasses all the analyses conducted in *displacement control.*

The entity of the vertical displacement in the mid-span in non-linear analyses is very beneath of the value of 1 millimeter. A vertical displacement in the mid-span has been applied in order to investigate as far as it is possible to push itself. Furthermore in some models it has been decided to apply a conceptually similar displacement to produce the same effect of lowering in the mid-span: a horizontal displacement is applied to the right support. For the purpose of the investigation, three attempt values of the displacement are proposed: 1, 2 and 3 mm. Each displacement has been applied with three different configuration described below:

1) vertical displacement in the mid-span applied on a set defined by two faces resulting from the cross section (Figure 3.13a);
2) vertical displacement in the mid-span applied on a reference point which has been bounded with the abovementioned set (Figure 3.13b);
3) horizontal displacement applied on the right support of the beam (Figure 3.13c).

Moreover, the displacement, is not applied instantaneously but through a linear monotonically increasing function.

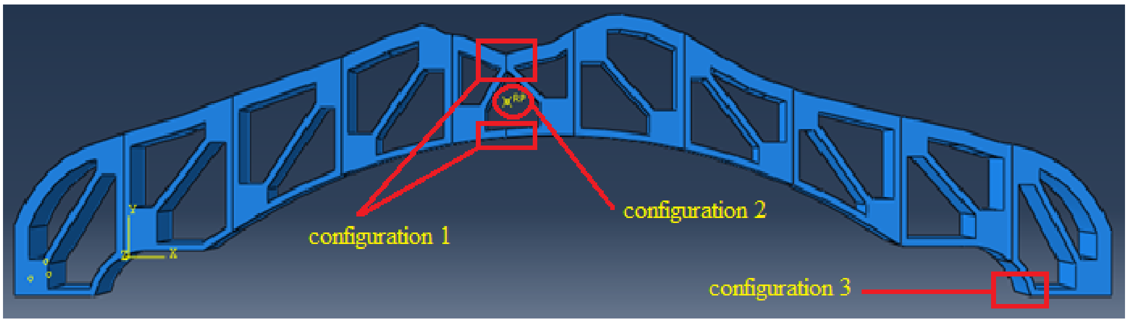

Figure 3.13 Localization of configuration on the beam

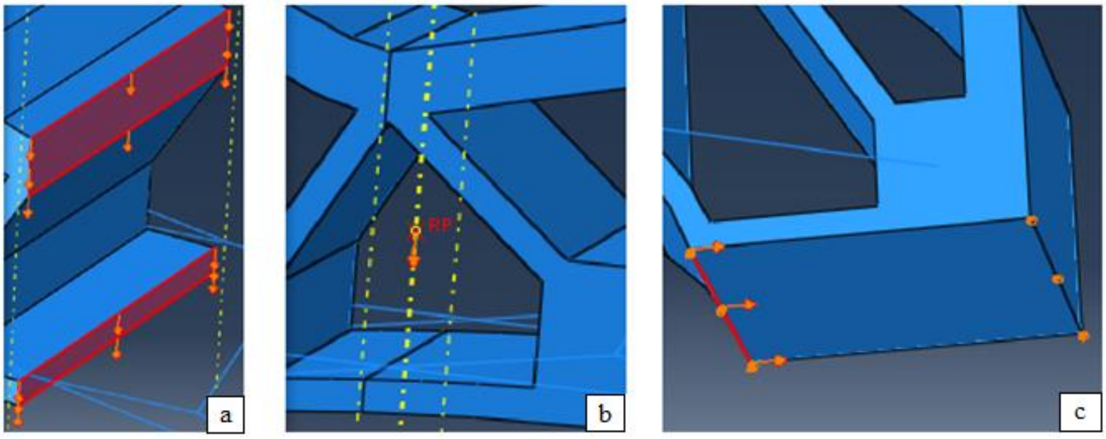

Figure 3.14 In order from the left the three methodologies for the displacement application

3.4 Mander constitutive behavior

The first step to implement the non-linear analyses is to define a non-linear constitutive behavior of the concrete. The Mander [8] constitutive behavior approach has been adopted.

3.4.1 The basic equation for monotonic compression loading

Mander et al. (1984) proposed a unified stress-strain approach for confined concrete applicable to both circular and rectangular shaped transverse reinforcement. The stress-strain model is based on an equations suggested by Popovics (1973) [8]. For a quasi-static strain rate and monotonic loading the longitudinal compressive concrete stress, fc, is given by:

$$fc = \frac{f'cc*x*r}{r-1+x'} \quad (3.1)$$

where $f_{cc} = f_{c0} * \left(-1.254 + 2.254 * \sqrt{1 + \frac{7.94*fi}{f_{c0}}} - 2 * \frac{fi}{f_{c0}}\right)$ is the compressive strength of the confined concrete.

$$x = \frac{\varepsilon_c}{\varepsilon_{cc}} \quad (3.2)$$

where ε_c = longitudinal compressive concrete strain

$$\varepsilon_{cc} = \varepsilon_{c0} * \left[1 + 5 * \left(\frac{f_{cc}}{f_{c0}} - 1\right)\right]$$

as suggested by Richart et al. (1928), where f_{c0} and ε_{c0} are the unconfined concrete strength and corresponding strain, respectively, and

$$r = \frac{E_c}{E_c - E_{sec}} \quad (3.3)$$

where

$$E_c = 5000 * \sqrt{f_{c0}} \text{ MPa} \quad \text{is the tangent modulus of elasticity of the concrete} \quad (3.4)$$

and

$$E_{sec} = \frac{f_{cc}}{\varepsilon_{cc}} \quad (3.5)$$

To define the stress-strain behavior of the cover concrete the part of the falling branch in the region where $\varepsilon_c > 2*\varepsilon_{c0}$ is assumed to be a straight line which reaches zero stress at the spalling strain, ε_{sp}[8].

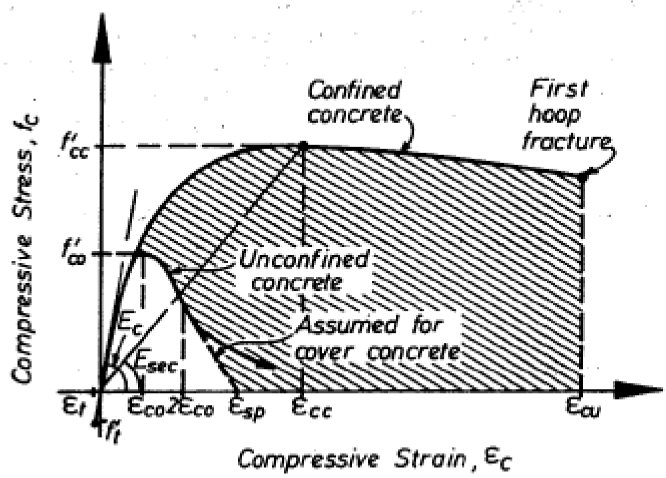

Figure 3.15 Stress-strain model proposed for monotonic loading of confined and unconfined concrete, taken from[8]

Since the 3D printed beam is an unconventional beam and it is also constituted by unconfined concrete, we need adapt the equations abovementioned to our case, then they become:

ε_{c0}= 0.002

$E_c \ = 5000 * \sqrt{f_{c0}}$

$E_{sec} = \frac{f_{cc}}{\varepsilon_{cc}}$

$$r = \frac{E_c}{E_c - E_{sec}}$$

the concrete strain ε_c have been imposed starting from 0.0001 to 0.0382 with an increment about 0.0001

$x = \frac{\varepsilon_c}{\varepsilon_{c0}}$ calculate for all values of ε_c (3.6)

$\sigma = \ f_{c0} * x * [\frac{r}{r-1+x^r}]$ calculate for all values of ε_c (3.7)

Subsequently the plastic strain is given by:

$\varepsilon_{plastic} = \ \varepsilon_{elastic} - \frac{\sigma}{E}$ (3.8) where

$\varepsilon_{elastic} = \varepsilon_c$

$$E = \frac{\sigma/3}{\varepsilon_{(\sigma/3)}} \tag{3.9}$$

In the following tables the numerical values of the parameters are represented:

Fco	ε_co	Ec	Esec	r	E
53,3	0,002	36503,4	26650	3,70464	36424,2

Table 3.3 Fundamental parameters

εc	x	σ	ε_plastic
0,00010	0,050	3,650	-2,2E-07
0,00020	0,100	7,300	-4,2E-07
0,00030	0,150	10,947	-5,5E-07
0,00040	0,200	14,587	-4,9E-07
0,00050	0,250	18,212	0
0,00060	0,300	21,809	1,25E-06
0,00070	0,350	25,361	3,74E-06
0,00080	0,400	28,845	8,09E-06
0,00090	0,450	32,234	1,5E-05
0,00100	0,500	35,497	2,55E-05
0,00110	0,550	38,596	4,04E-05
0,00120	0,600	41,492	6,09E-05
0,00130	0,650	44,146	8,8E-05
0,00140	0,700	46,517	0,000123
0,00150	0,750	48,569	0,000167
0,00155	0,775	49,466	0,000192
0,00160	0,800	50,273	0,00022
0,00165	0,825	50,987	0,00025
0,00170	0,850	51,606	0,000283
0,00175	0,875	52,129	0,000319
0,00180	0,900	52,554	0,000357
0,00185	0,925	52,883	0,000398

0,01180	5,900	1,7752	0,011756
0,01220	6,100	1,775209	0,012159
0,01260	6,300	1,775218	0,012563
0,01300	6,500	1,775227	0,012966
0,01340	6,700	1,775237	0,013368
0,01380	6,900	1,775246	0,013771
0,01420	7,100	1,775246	0,014173
0,01460	7,300	1,775246	0,014575
0,01500	7,500	1,775246	0,014977
0,01540	7,700	1,775246	0,015378
0,01580	7,900	1,775246	0,01578
0,01620	8,100	1,775246	0,016181
0,01660	8,300	1,775246	0,016582
0,01700	8,500	1,775246	0,016983
0,01740	8,700	1,775246	0,017384
0,01780	8,900	1,775246	0,017785
0,01820	9,100	1,775246	0,018186
0,01860	9,300	1,775246	0,018587
0,01900	9,500	1,775246	0,018988
0,01940	9,700	1,775246	0,019388
0,01980	9,900	1,775246	0,019789
0,02020	10,100	1,775246	0,02019
0,02060	10,300	1,775246	0,02059

0,00190	0,950	53,116	0,000442
0,00195	0,975	53,254	0,000488
0,00200	1,000	53,300	0,000537
0,00205	1,025	53,255	0,000588
0,00210	1,050	53,124	0,000642
0,00215	1,075	52,909	0,000697
0,00220	1,100	52,616	0,000755
0,00225	1,125	52,247	0,000816
0,00230	1,150	51,809	0,000878
0,00235	1,175	51,306	0,000941
0,00240	1,200	50,744	0,001007
0,00245	1,225	50,126	0,001074
0,00250	1,250	49,460	0,001142
0,00255	1,275	48,750	0,001212
0,00260	1,300	48,000	0,001282
0,00265	1,325	47,217	0,001354
0,00270	1,350	46,405	0,001426
0,00275	1,375	45,568	0,001499
0,00280	1,400	44,711	0,001572
0,00285	1,425	43,838	0,001646
0,00290	1,450	42,953	0,001721
0,00295	1,475	42,060	0,001795
0,00300	1,500	41,161	0,00187
0,00340	1,700	34,096	0,002464
0,00380	1,900	27,819	0,003036
0,00420	2,100	22,627	0,003579
0,00460	2,300	18,472	0,004093
0,00500	2,500	15,187	0,004583
0,00540	2,700	12,593	0,005054
0,00580	2,900	10,536	0,005511
0,00620	3,100	8,894	0,005956
0,00660	3,300	7,572	0,006392
0,00700	3,500	6,498	0,006822
0,00740	3,700	5,618	0,007246
0,00780	3,900	4,890	0,007666
0,00820	4,100	4,284	0,008082
0,00860	4,300	3,775	0,008496
0,00900	4,500	3,344	0,008908

0,02100	10,500	1,775246	0,020991
0,02140	10,700	1,775246	0,021391
0,02180	10,900	1,775246	0,021792
0,02220	11,100	1,775246	0,022192
0,02260	11,300	1,775246	0,022592
0,02300	11,500	1,775246	0,022993
0,02340	11,700	1,775246	0,023393
0,02380	11,900	1,775246	0,023793
0,02420	12,100	1,775246	0,024194
0,02460	12,300	1,775246	0,024594
0,02500	12,500	1,775246	0,024994
0,02540	12,700	1,775246	0,025394
0,02580	12,900	1,775246	0,025795
0,02620	13,100	1,775246	0,026195
0,02660	13,300	1,775246	0,026595
0,02700	13,500	1,775246	0,026995
0,02740	13,700	1,775246	0,027395
0,02780	13,900	1,775246	0,027796
0,02820	14,100	1,775246	0,028196
0,02860	14,300	1,775246	0,028596
0,02900	14,500	1,775246	0,028996
0,02940	14,700	1,775246	0,029396
0,02980	14,900	1,775246	0,029796
0,03020	15,100	1,775246	0,030196
0,03060	15,300	1,775246	0,030597
0,03100	15,500	1,775246	0,030997
0,03140	15,700	1,775246	0,031397
0,03180	15,900	1,775246	0,031797
0,03220	16,100	1,775246	0,032197
0,03260	16,300	1,775246	0,032597
0,03300	16,500	1,775246	0,032997
0,03340	16,700	1,775246	0,033397
0,03380	16,900	1,775246	0,033797
0,03420	17,100	1,775246	0,034197
0,03460	17,300	1,775246	0,034598
0,03500	17,500	1,775246	0,034998
0,03540	17,700	1,775246	0,035398
0,03580	17,900	1,775246	0,035798

0,00940	4,700	2,978	0,009318
0,00980	4,900	2,664	0,009727
0,01020	5,100	2,393	0,010134
0,01060	5,300	2,158	0,010541
0,01100	5,500	1,954	0,010946
0,01140	5,700	1,775	0,011351

0,03620	18,100	1,775246	0,036198
0,03660	18,300	1,775246	0,036598
0,03700	18,500	1,775246	0,036998
0,03740	18,700	1,775246	0,037398
0,03780	18,900	1,775246	0,037798
0,03820	19,100	1,775246	0,038198

Table 3.4 Compression behavior curve parameters

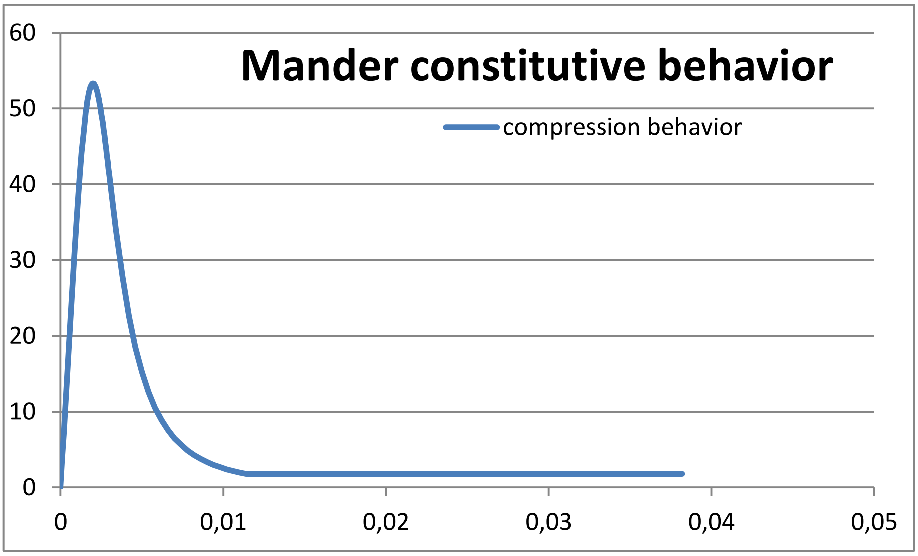

Figure 3.16 Mander constitutive behavior, compression behavior curve

3.4.2 The tensile constitutive behavior curve

For the tensile behavior a linear approach has been adopted, a straight line has been implemented starting from the tensile characteristic stress of the concrete to the 20% of that, with a final plastic strain equal to 5‰. Then, the first step has been calculate the tensile characteristic stress of the concrete starting from the compression resistance adopted:

$$f_{ck} = 53.3\ MPa$$

$$f_{ctm} = 0{,}3 * f_{ck}^{2/3} = 4{,}25\ MPa$$

$$f_{ctk} = 0{,}7 * f_{ctm} = 2{,}975\ MPa$$

$20\% * f_{ctk} = 0{,}2 * 2{,}975 = 0{,}595\ MPa$

The points for the straight line are:

(2,975 ; 0)   (0,595 ; 0,005)

and the equation is

$y = -0{,}0021 * x + 0{,}0062475$

where y represented the strain values and x represented the stress value.

In the following table the numerical values are reported.

stress	plastic strain
0	0
2,92948	9,55786E-05
2,914491526	0,000127068
2,894322035	0,000169424
2,874152544	0,00021178
2,853983053	0,000254136
2,833813562	0,000296492
2,813644071	0,000338847
2,79347458	0,000381203
2,773305089	0,000423559
2,753135598	0,000465915
2,732966107	0,000508271
2,712796616	0,000550627
2,692627125	0,000592983
2,672457634	0,000635339
2,652288143	0,000677695
2,632118652	0,000720051
2,611949161	0,000762407
2,59177967	0,000804763
2,571610179	0,000847119
2,551440688	0,000889475
2,531271197	0,00093183
2,511101706	0,000974186
2,490932215	0,001016542
2,470762724	0,001058898
2,450593233	0,001101254
2,430423742	0,00114361
2,410254251	0,001185966
2,39008476	0,001228322
2,087542	0,001864
2,067373	0,001906
2,047203	0,001948
2,027034	0,001991
2,006864	0,002033
1,986695	0,002075
1,966525	0,002118
1,946356	0,00216
1,926186	0,002203
1,906017	0,002245
1,885847	0,002287
1,865678	0,00233
1,845509	0,002372
1,825339	0,002414
1,80517	0,002457
1,785	0,002499
1,764831	0,002541
1,744661	0,002584
1,724492	0,002626
1,704322	0,002668
1,684153	0,002711
1,663983	0,002753
1,643814	0,002795
1,623644	0,002838
1,603475	0,00288
1,583305	0,002923
1,563136	0,002965
1,542966	0,003007
1,522797	0,00305
1,220254	0,003685
1,200085	0,003727
1,179915	0,00377
1,159746	0,003812
1,139576	0,003854
1,119407	0,003897
1,099237	0,003939
1,079068	0,003981
1,058898	0,004024
1,038729	0,004066
1,018559	0,004109
0,99839	0,004151
0,97822	0,004193
0,958051	0,004236
0,937881	0,004278
0,917712	0,00432
0,897542	0,004363
0,877373	0,004405
0,857203	0,004447
0,837034	0,00449
0,816864	0,004532
0,796695	0,004574
0,776525	0,004617
0,756356	0,004659
0,736186	0,004702
0,716017	0,004744
0,695848	0,004786
0,675678	0,004829
0,655509	0,004871

2,369915269	0,001270678
2,349745778	0,001313034
2,329576287	0,00135539
2,309406796	0,001397746
2,289237305	0,001440102
2,269067814	0,001482458
2,248898323	0,001524814
2,228728832	0,001567169
2,208559341	0,001609525
2,18838985	0,001651881
2,168220359	0,001694237
2,148050868	0,001736593
2,127881377	0,001778949
2,107711886	0,001821305
1,502627	0,003092
1,482458	0,003134
1,462288	0,003177
1,442119	0,003219
1,421949	0,003261
1,40178	0,003304
1,38161	0,003346
1,361441	0,003388
1,341271	0,003431
1,321102	0,003473
1,300932	0,003516
1,280763	0,003558
1,260593	0,0036
1,240424	0,003643
0,635339	0,004913
0,61517	0,004956
0,595	0,004998
0,595	0,005089
0,595	0,00518
0,595	0,005271
0,595	0,005362
0,595	0,005453
0,595	0,005545
0,595	0,005636
0,595	0,005727
0,595	0,005818
0,595	0,005909

Table 3.5 Tensile behavior curve parameters

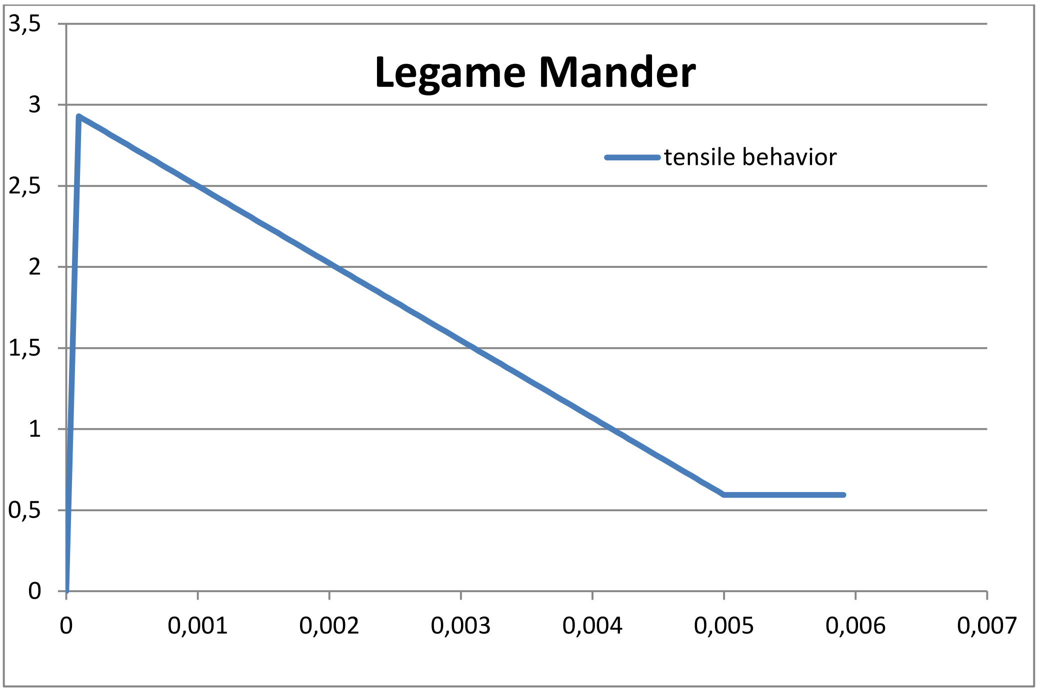

Figure 3.17 Mander constitutive behavior, tensile behavior curve

To realize the graph about the tensile concrete behavior, it needed to introduce the elastic branch. In order to obtain this, the equation of the straight line of the elastic branch in the graph, representing the compression behavior was found. Systematizing the two equations, the meeting point, dividing the elastic branch and the softening one, was determined.

3.5 Simulation of a tensile test

In order to verify the effectiveness of the material just implemented, a simulation of a tensile test has been conducted on a concrete cube which has the edge size equal to 10 cm. The cube is bounded on three faces with the following constraints:

- X-symmetric, in which U1 = UR2 = UR3 = 0;
- Y-symmetric, in which U2 = UR1 = UR3 = 0;
- Z-symmetric, in which U3 = UR2 = UR1 = 0.

A controlled displacement has been applied to urge the cube; four displacement cases have been employed in which the value of the displacement change each time with the following scheme:

1) 0.25 mm
2) 0.5 mm
3) 0.75 mm
4) 1 mm

Figure 3.17 shows the boundary conditions applied to the cube and in particular the arrows in the z-direction represent the direction of the imposed displacement. Figure 3.18, instead, shows a plot of the deformed model highlighting the entity of the displacement in the z-direction. Furthermore, the graphics reported below represent the constitutive behavior curve (stress-strain) for each displacement case.

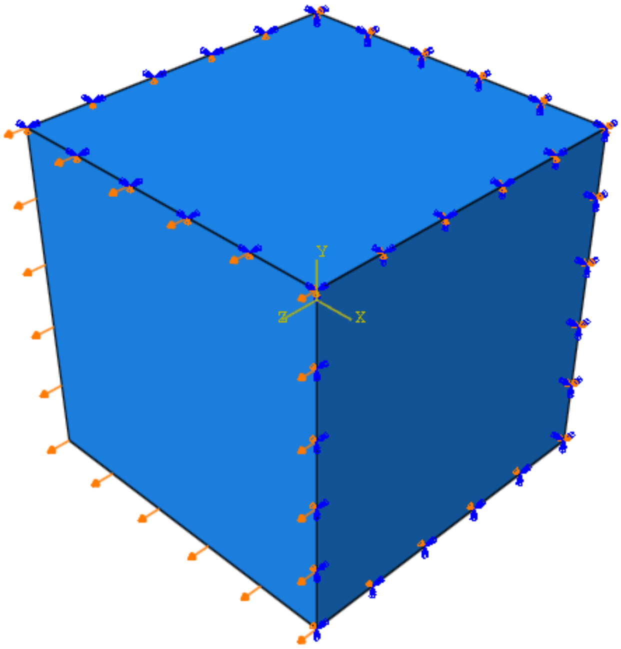

Figure 3.18 Boundary conditions on the cube, the arrows in z-direction represent the displacement direction

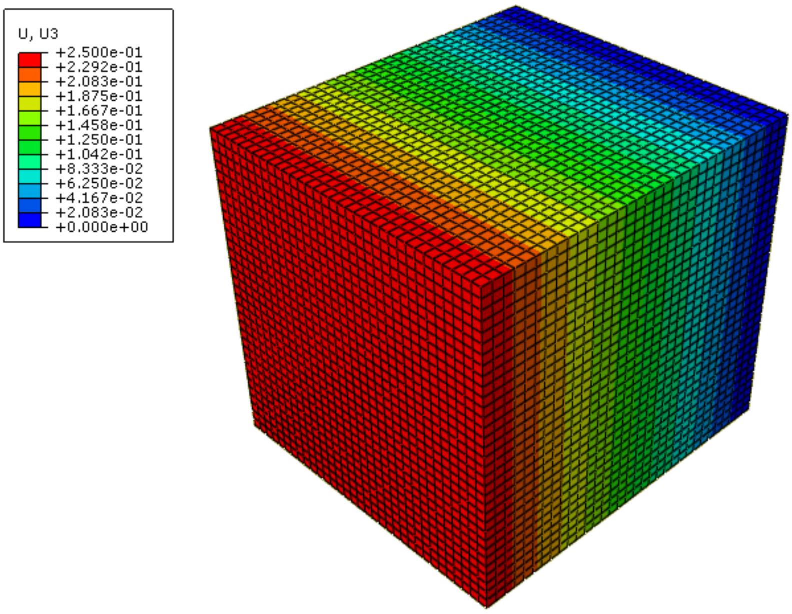

Figure 3.19 Contour plot of the displacement U3 in the first load case

The final scope of these tests is to obtain a stress-strain graphics to compare with the Mander [8] constitutive behavior implemented in the analyses. To do this, it was necessary to plot the stress and strain variables in function of time separately and then combine them in a single graph to obtain the desired constitutive behavior. The graphics are sorted by increasing imposed displacement:

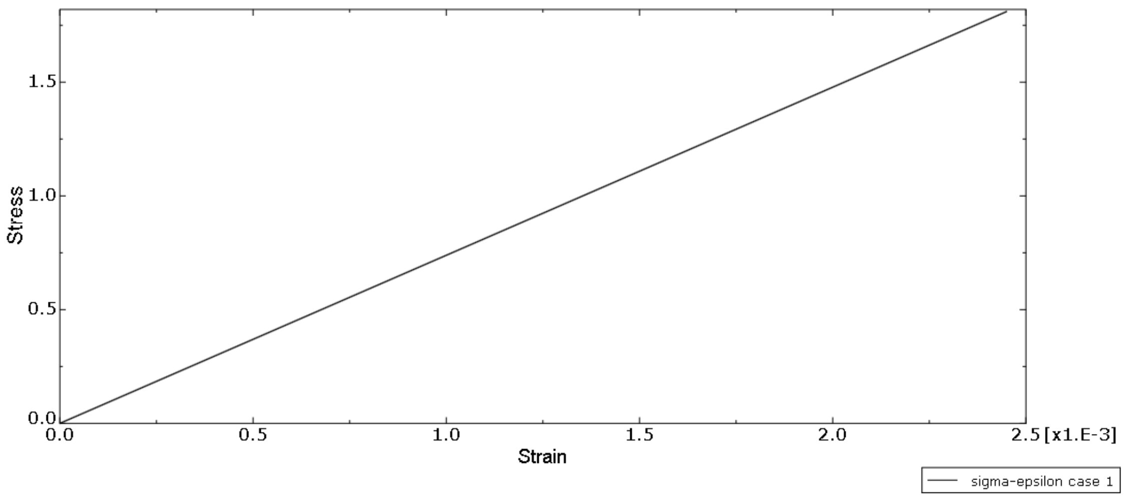

Figure 3.20 Stress-strain graph about case 1

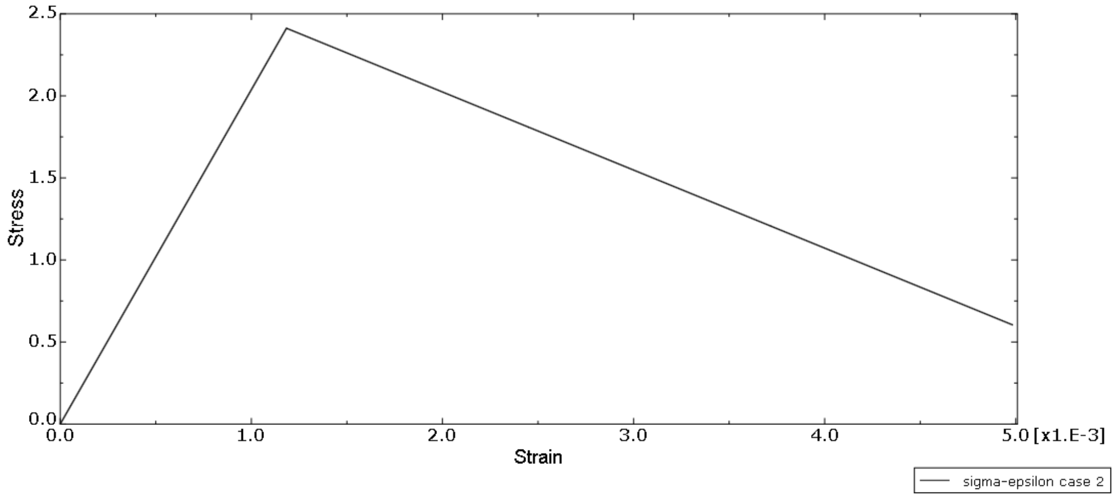

Figure 3.21 Stress-strain graph about case 2

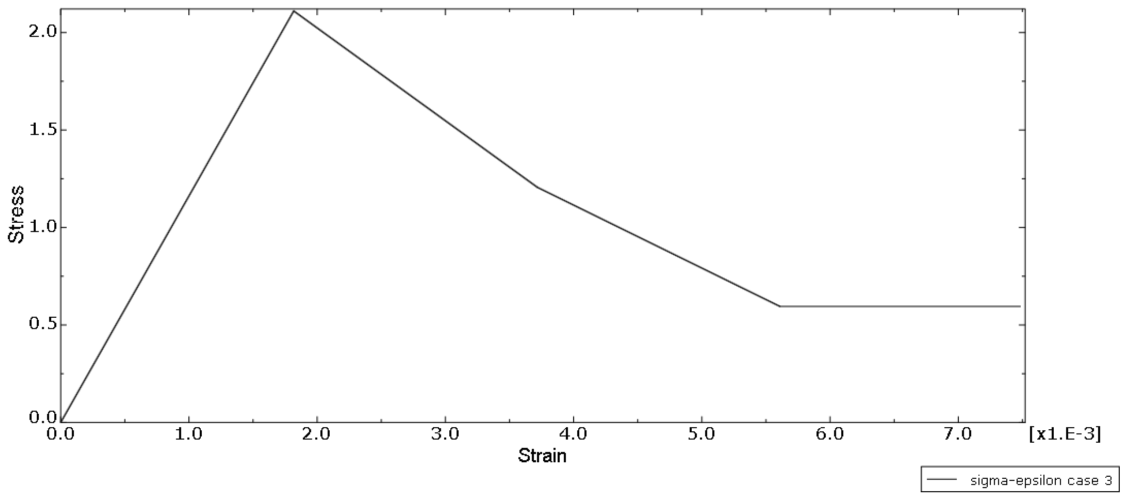

Figure 3.22 Stress-strain graph about case 3

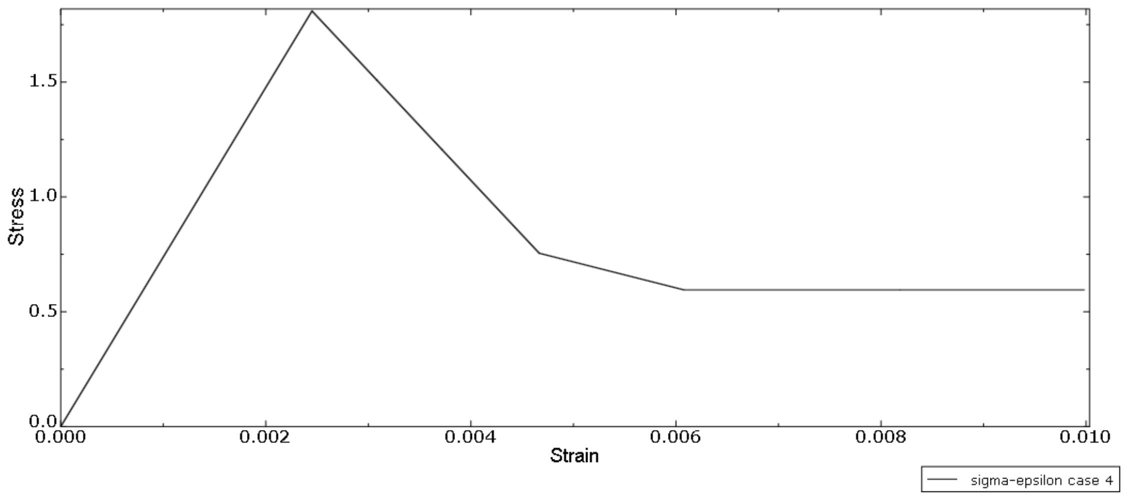

Figure 3.23 Stress-strain graph about case 4

How we can see from the graphics, while the displacement imposed increases, the stress-strain graph changes his shape. In particular we can see the transition from elastic behavior to the elastic-plastic behavior.

A further graph depicts the envelop between the four obtained graphics, in order to show the shape changing related to the displacement entity:

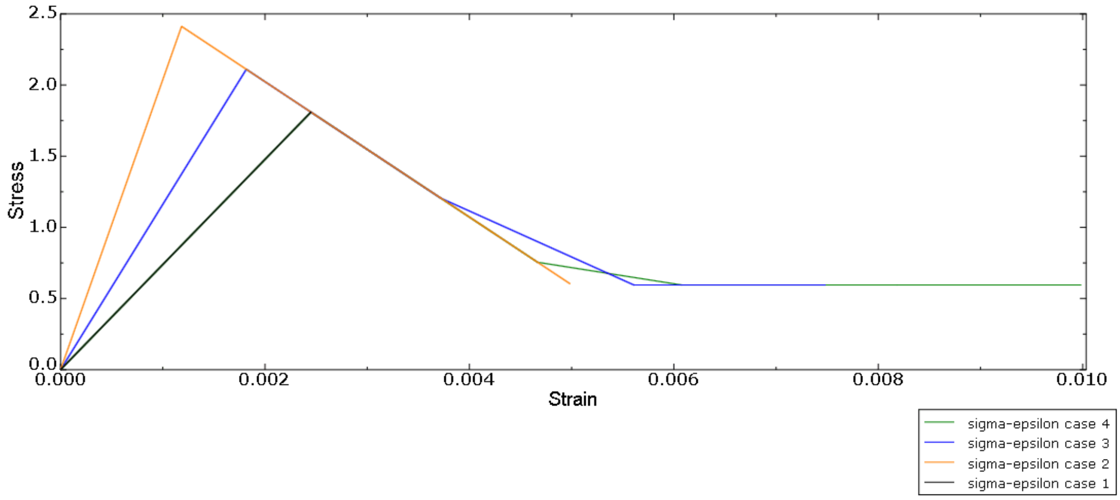

Figure 3.24 Envelope

3.6 The printing machine

The printer used to build the aforementioned beams was made by the WASP group, one of the most forefront Italian enterprise. The external frame of the machine is composed by three vertical uprights assembled with diagonals metal bands to ensure stability. Thus, the print area obtained is a triangle having each side of about 4 m. On top of the uprights three braces are connected, one on each upright, supporting the printing head. The last one is formed by a conical container with a capacity of 20 liters which, through the braces movement along the uprights, can be moved horizontally and vertically and can reach a height of 1.5 m above the ground. The fresh concrete content inside the print head is extruded from an endless screw through a nozzle, which can have a variable diameter. The printing head movement is controlled by a control unit that works with an STL and software that provides to the printer the following inputs:

- the path that the head should follow during the printing process of each layer;
- the height of the layer;
- the print head speed

The element is printed layer by layer in vertical direction, orthogonal to the element design plane. A series of parameters influences the thickness of the printed line, such as:

- viscosity of the fluid;
- extrusion force;
- nozzle diameter;
- layer thickness;
- print speeds.

The optimal balance between these elements also guarantees the stability of the layer just been printed, and the capability to sustain the weight of subsequent layers.

Particular attention was paid to the viscosity of the fresh mortar, as the demand of making the printing material extrudable and buildable. In addition, it was necessary a great strength of concrete to balance the weakness in the connection points between layers. Finally the concrete must have a small aggregate size in relation to nozzle diameter (25 mm).

The mortar composition was studied by the Department of Structures for Engineering and Architecture of the University Federico II of Naples through mix-design techniques which lead to the definition of optimal percentage of each component. It was also added a small percentage of polypropylene short fibers, to increase viscosity.

To test the mechanical characteristics of concrete, during the printing phase, some samples were taken, to carried out the mono-axial compression tests and to obtain the characteristic resistances R_{ck} and F_{ck} whose values are standard. Moreover, some cylindrical specimens were made through the printing machine, to compare this result with the previous ones. We can note that the compression resistance of the printed material is about less than 16%. Maybe this discrepancy is caused by:

- an imperfect bond between the layers that can initiate the failure of the specimen;
- a reduced thickness of the wall, that can lead to a stress concentration and may trigger the failure of the specimen.

Considering this, it is important careful evaluation of all physical and chemical properties of the material before the printing phase.

Figure 3.24 reported in the next page shows the printer machine.

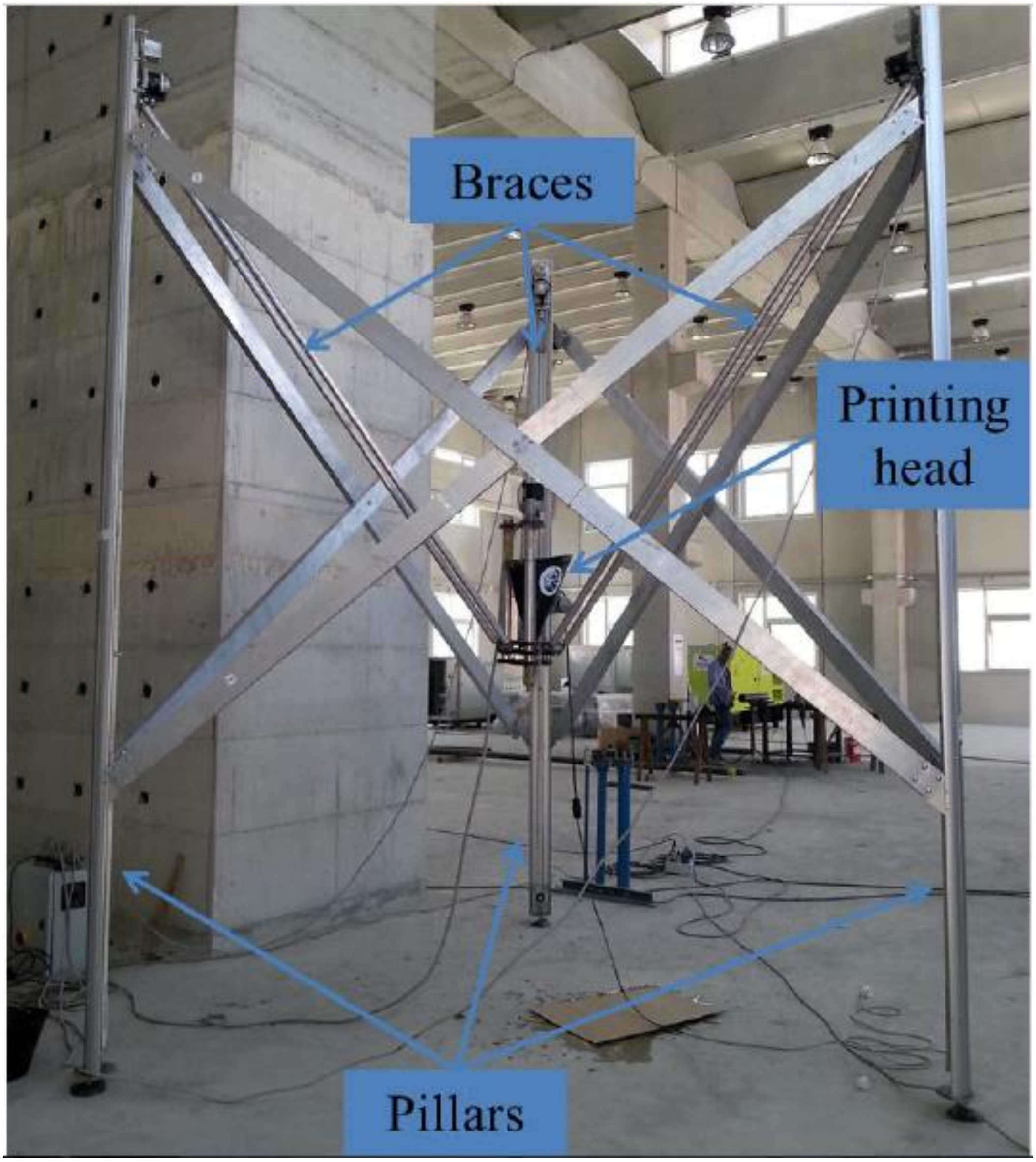

Figure 3.25 Printer machine

The next figure represents the printing process of the elements of the straight beam and the first phase of the assembly procedure in which the elements are positioned next, each to one another.

Figure 3.26 Printing and assembly processes of the straight beam

A lateral and front view of the assembled beam are reported below:

Figure 3.27 Lateral view

Figure 3.28 Front view

The last figures depicted the curved beam printing and the final assembly:

Figure 3.29 Printing process

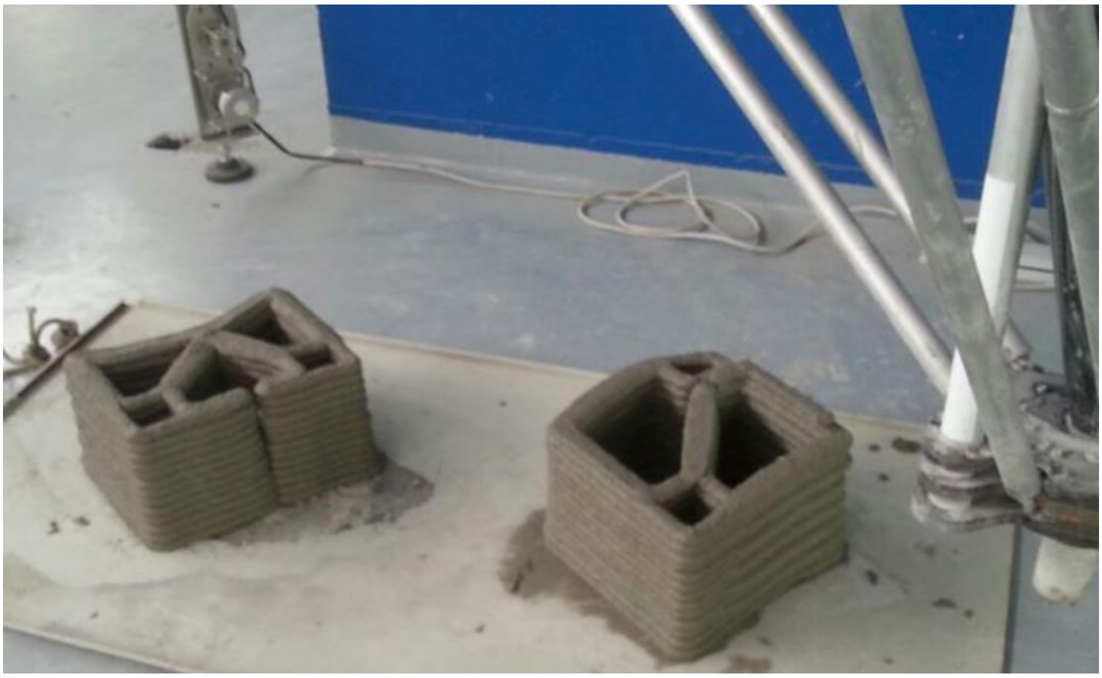

Figure 3.30 Two printed elements of the curved beam

Figure 3.31 Assembly phase of the curved beam

Figure 3.32 Curved beam assembled

4 Numerical analyses

This chapter will describe the model construction, that is approximately the same for all models, and subsequently all the analyses with relative boundary conditions, loads applied and the most significant plot of stress and displacement quantities will be reported.

4.1 Straight beam

This paragraph shows the numerical model and two plots of the stresses in the concrete elements and in the steel bars about the straight beam.

It must be remembered that only some results about straight beam will be reported because the whole work had already finished before the beginning of this project. Concerning the curved beam, the main topic of this document and on which the author worked about, both the step of numerical analysis and project step from the preliminary test will be reported.

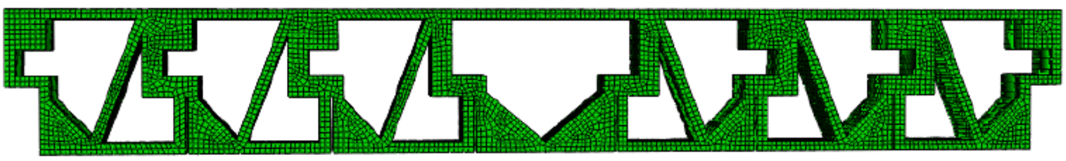

Figure 4.1 Numerical Model

Vertical supports are been modelled on the two sides of the beam with a total span of 3.2 m and a distributed uniform load equal to 0.9 Kn/m was applied for the analyses. The figure reports the deformation path and the axial stress in the steel bars:

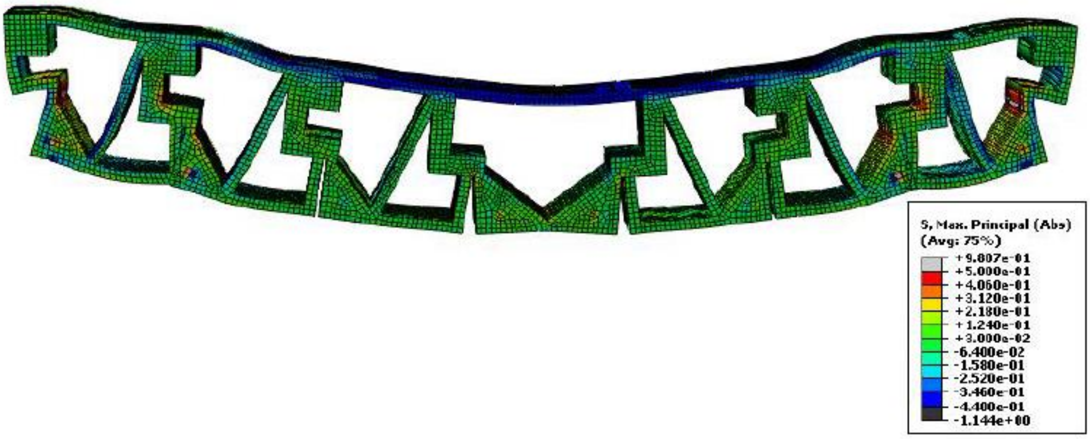

Figure 4.2 Deformation Path with the plot of the max stress component

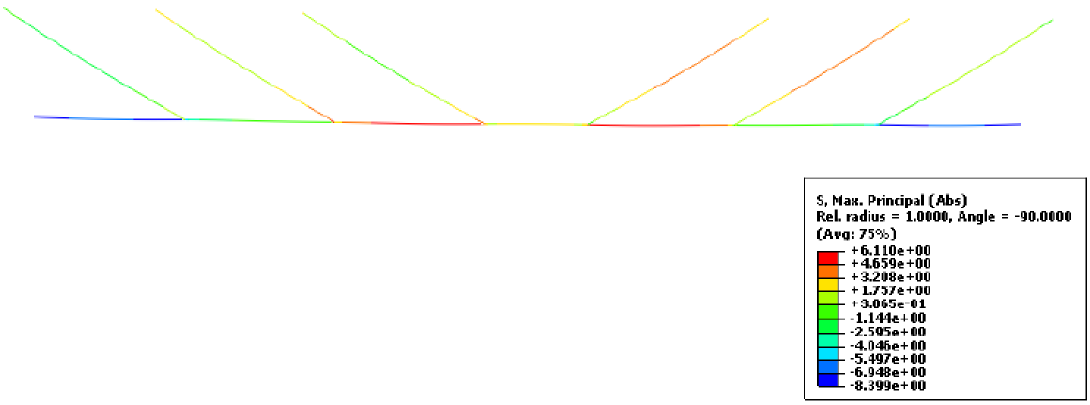

Figure 4.3 Axial stress in steel bars

Finally, the beam has been printed element by element that were subsequently assembled with the help of the steel bars that have been fixed in their hole with an epoxy high strength resin.

It can be seen on the basis of the results that both the inner stresses of concrete and reinforcement bars are acceptable values. Therefor the beam does not exhibit some particular resistance and deformation problems, under its uniquely self-weight load.

4.2 Model construction

4.2.1 Abaqus/CAE software

Abaqus/CAE is a suite of powerful engineering simulation programs based on the finite element method. It contains an extensive library of element that can model any geometry, furthermore it allows to import geometry from many different CAD software packages. Using this program we are able to use various different material models to simulate the behavior of most typical engineering materials like metals, rubber, polymers, reinforced concrete, geotechnical materials and other more.

Designed as a general-purpose simulation tool, Abaqus/CAE can be used to study more than just structural problems. It can simulate problems in such diverse areas as mass diffusion, thermal management of electrical components, acoustics, moils mechanics and piezoelectric analyses. Furthermore it offers a large range of capabilities for simulation linear and non-linear applications; problems with multiple components are modelled by associating the geometry defining each component with its material model and the appropriate component interaction.

Abaqus/CAE automatically chooses appropriate load increment and convergence tolerance in a non-linear analyses, and continually adjusts them during the analysis to ensure that an accurate solution is obtained [9].

4.2.2 Part module

In the Part module we are able to design any geometry for the model construction or to import a sketch designed with other Cad software. In this module we create the model that may be the whole model if is a simple geometry or we can construct a single part of the model that will be assembled in the assembly module [10]. In our case the second procedure has been chosen because of the complexity of the geometry, then, a single element part has been create for each element importing a sketch from AutoCad software. In the end there are ten parts for the concrete beam and one part for the rebar system.

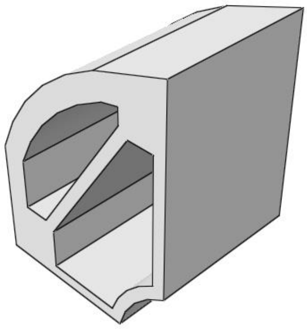

Figure 4.4 Example of a single element part

4.2.3 Property module

In this module we are able to assign the property of the parts like the material and the section. Before editing the section properties we must define the material that will be assigned to the corresponding section. A linear-elastic constitutive behavior has been used for both materials and whose characteristics are already reported in table 3.1 and 3.2

For the non-linear analyses a non-linear constitutive behavior has been implemented for the concrete that is described in chapter 3.

After that, we are able to create a section for each element type, which in this case are three:

- Concrete: solid and homogeneous section type
- Steel brackets: truss section type with 201 mm^2 of cross section
- Steel tie: beam section type with circular profile shape and 201 mm^2 of cross section

Then these sections have been assigned to their corresponding parts.

4.2.4 Assembly module

The first step to obtain a global assembly of the parts is that create a part instance for each part existing in the model. Part instances can be thought of as representation of the original parts. Each part is oriented in its own coordinate system and is independent from the other parts in the model. Although a model contains several parts, only one assembly can be defined [10]. The geometry of the assembly is defined by creating instances of a part and then positioning the instances relative to each other in a global coordinate system. An instance may be independent or dependent.

In this phase also the surfaces, in particular those of both side of each concrete element, the global front and rear surface of the entire model and the rebar nodes set, necessary to constrain blocks and bars in mutual connection have been created.

Below the whole assembly and an example of vertical surface are represented:

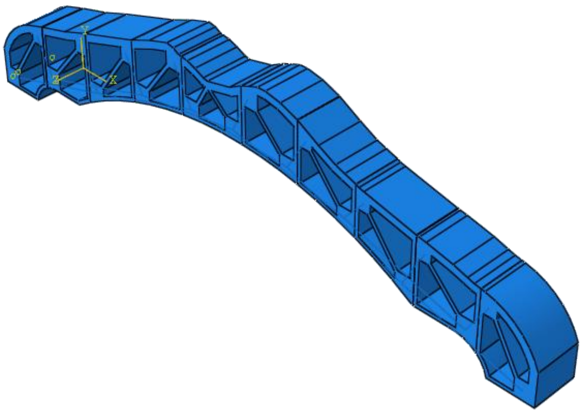

Figure 4.5 Global assembly

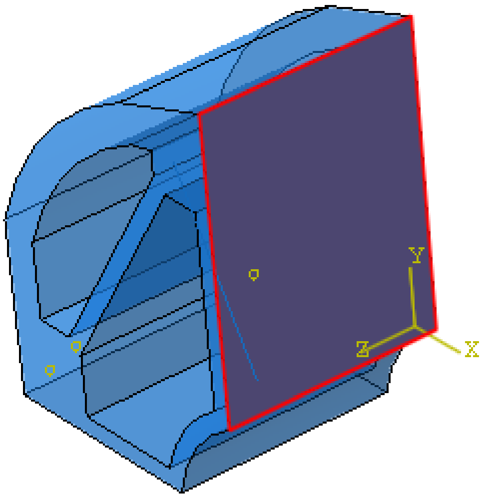

Figure 4.6 Vertical surface

4.2.5 Step module

The step module has been used to perform the following tasks:

- To create analysis steps: within a model we define a sequence of one or more analysis steps. The step sequence provides a convenient way to capture changes in the loading and boundary conditions of the model, changes in the way, parts of the model interact with each other, the removal or addition of parts, and any other changes that may occur in the model during the course of the analysis. In addition, steps allow to change the analysis procedure, the data output, and various controls.
- To specify output requests: Abaqus/CAE writes output from the analysis to the output database; we can specify the output by creating output requests that are propagated to subsequent analysis steps. An output request defines which variables will be output during an analysis step, from which region of the model they will be output, and at what rate they will be output.

In our case two steps have been created: the initial one and the step-1 in which the load applied and the boundary conditions used have been specified [10].

4.2.6 Interaction module

In this module Abaqus/CAE allows to define the interaction type between the regions of the model. There are many kind of interactions like as general contact, surface-to-surface contact, fluid cavity, fluid exchange and others. In this phase we are also able to define the constraints between parts or region of the model, like as tie, rigid body and others.

In our analyses the tie constraint on the first group of analyses and the contact interaction on the second one have been employed. The two typologies are described subsequently:

- Tie: A tie constraint allows to fuse together two regions even though the meshes created on the surfaces of the regions may be dissimilar.
- Contact: A contact interaction property can define tangential behavior (friction and elastic slip) and normal behavior (hard, soft, or damped contact and separation). For the tangential behavior a friction coefficient equal to 0,45 has been defined. In addition, a contact property can contain information about

damping, thermal conductance, thermal radiation, and heat generation due to friction. A contact interaction property can be referred to by a general contact, surface-to-surface contact, or self-contact interaction [10].

4.2.7 *Load module*

In the load module the load applied and the boundary conditions have been defined. For these analyses only gravity load has been applied while three boundary conditions have been employed that are combined each other to obtain the desired constraints on the beam:

1) Zipper: applied on the right edge of the bottom face of the first element in which the displacements U1, U2 and U3 are equal to zero;
2) Support: applied on the left edge of the bottom face of the last element in which the displacements U2 and U3 are equal to zero;
3) BC1: applied on the left edge of the bottom face of the first element and on the right edge of the bottom face of the last element in which the displacement U3 is equal to zero.

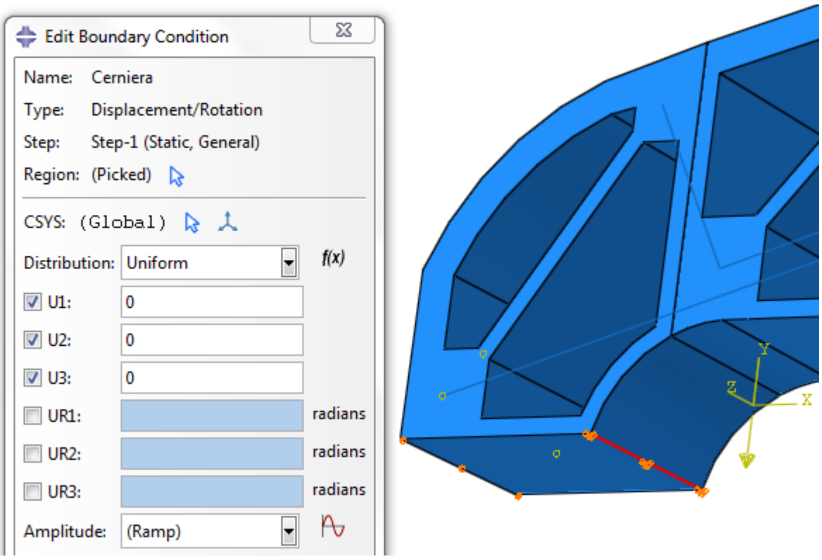

Figure 4.7 Example of boundary condition editor

In this module, a controlled displacement is also defined for non-linear analyses, which is implemented through a temporal function called Amplitude.

4.2.8 Mesh module

The mesh module allows to generate meshes on parts and assemblies created within Abaqus/CAE. We must specify that the parts are associated with dependent instances, so when we mesh one part, Abaqus/CAE applies the same mesh to each dependent instance in the assembly. To mesh the assembly the seeding procedure has been used in which seeds, that are markers, are placed along the edges of a region to specify the target mesh density in that region. A free mesh technique has been adopted and the approximately size of the elements is equal to 15 mm [10].

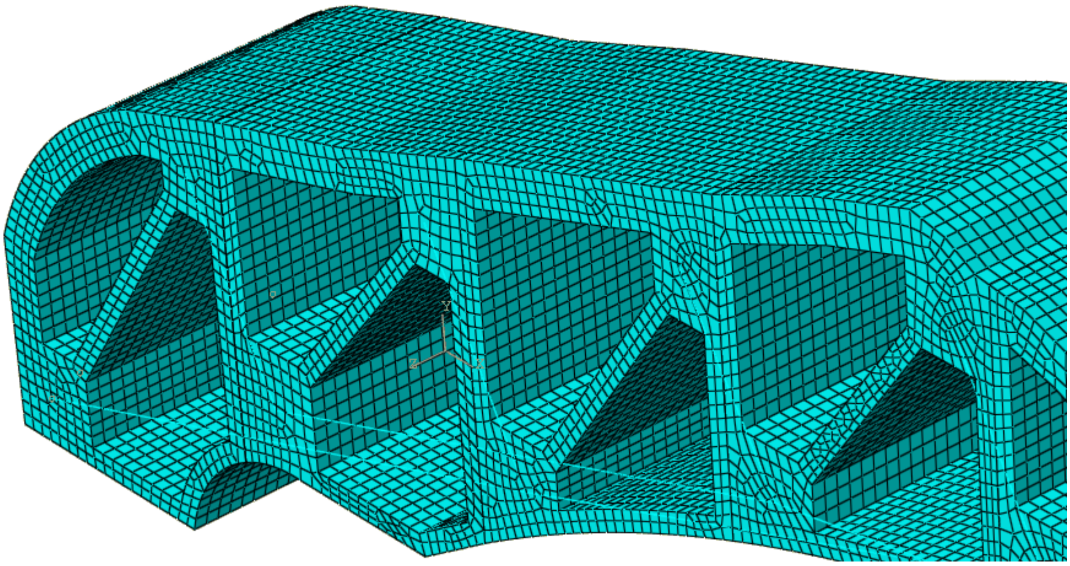

Figure 4.8 Mesh completed

4.2.9 Job module

In the job module we are able to analyze the model. The basic steps for analyzing the model are:

a) To create and to configure an analysis job: in this phase Abaqus/CAE asks to name the new job and to associate it with a model selected from the model database or with an existing input file. We are able to select any model that exists in the database. The job editor allows to configure the job settings;
b) To write the input file: submitting a job associated with a model for analysis, Abaqus/CAE first generates an input file representing the model and then

Abaqus/Standard, Abaqus/Explicit, or Abaqus/CFD performs the analysis using the contents of this file;

c) To submit the job for analysis: as the analysis progresses, Abaqus/CAE displays information from the status, data, log, and message files in the job monitor dialog box. After the job is completed, we can display results from the output database in the visualization module [10].

4.2.10 Visualization module

Finally, this module allows to display the intermediate and final results of the analysis, using multiple tools and functions, which allow, for example, to plot the stress state in a section and the variation over time of the displacement component in a particular point, to use the appropriate scale of deformations to better read the displacements and to see the evolution of the model through animations[10].

4.3 *Curved beam, preliminary tests*

In according to the procedure adopted, the configurations descripted in chapter three have been imported in the Abaqus/CAE software to investigate the approximately behavior of the beam.

All three configurations are characterized with two load configurations: the first consists in the gravity load, the weight of the beam; the second, instead, consists in the full section beam weight, (about 9,29 Kn) divided into eighteen concentrated forces and applied on the top side of the beam.

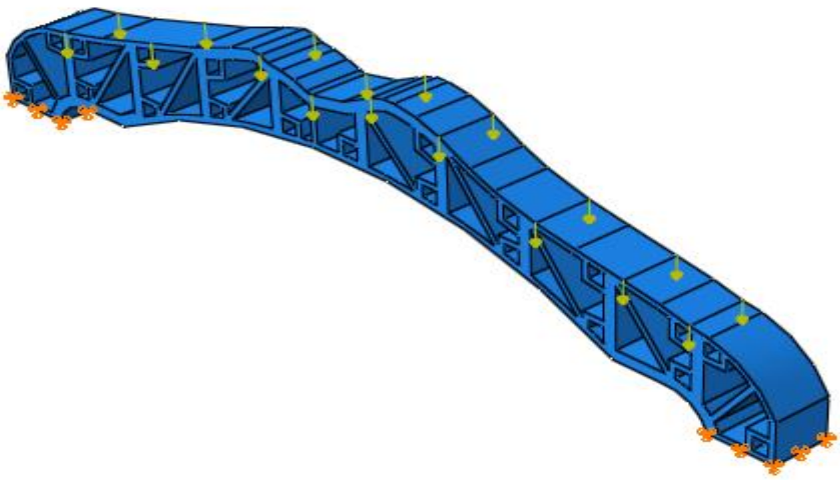

Figure 4.9 Example of the application load procedure

The boundary conditions adopted were zipper-zipper applied on the bottom face of the external elements in which displacements U1, U2 and U3 has been bounded.

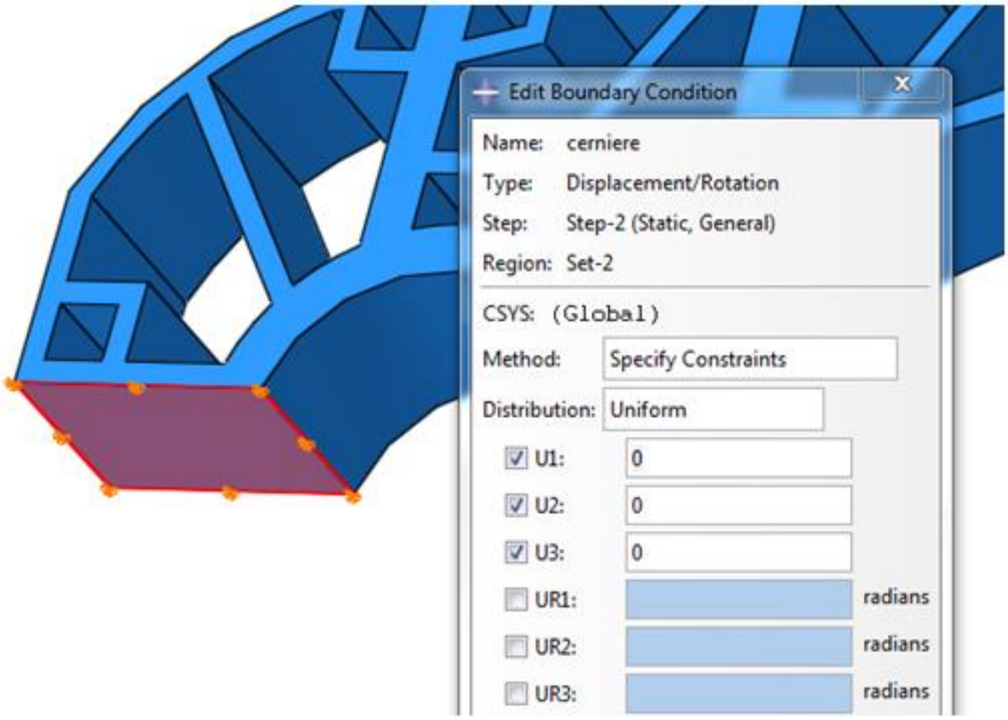

Figure 4.10 Boundary conditions

Furthermore, we must specify that the model analyzed was a monolithic beam because there was not any particular constraints between the elements (such as contact or tie constraints), indeed the whole model from Cad has been imported and not the singular elements.

ANALYSIS 1

Configuration 1

Boundary conditions: zipper-zipper

Load applied: gravity + concentrated forces on top side of the beam

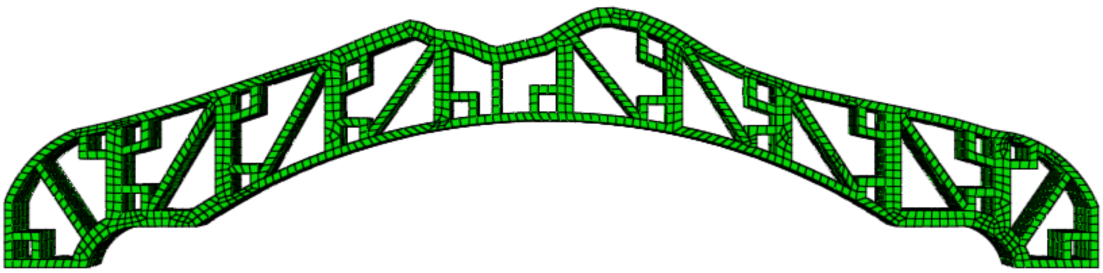

Figure 4.11 Configuration 1, numerical model

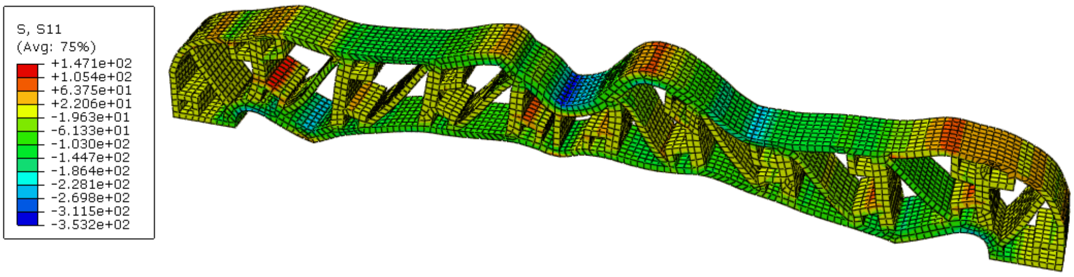

Figure 4.12 Configuration 1, concrete stress S11

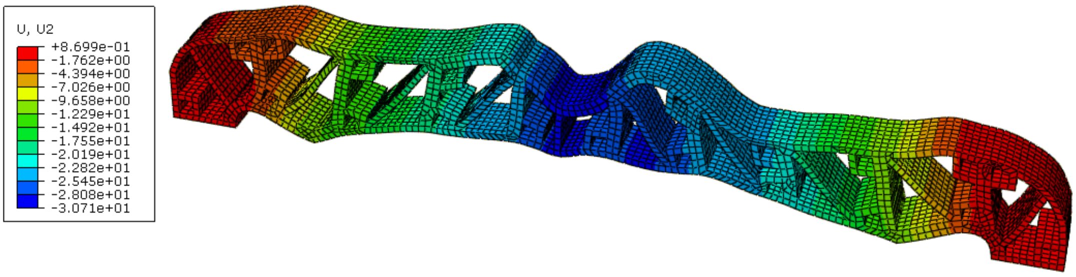

Figure 4.13 Configuration 1, displacement U2

ANALYSIS 2

Configuration 2

Boundary conditions: zipper-zipper

Load applied: gravity + concentrated forces on top side of the beam

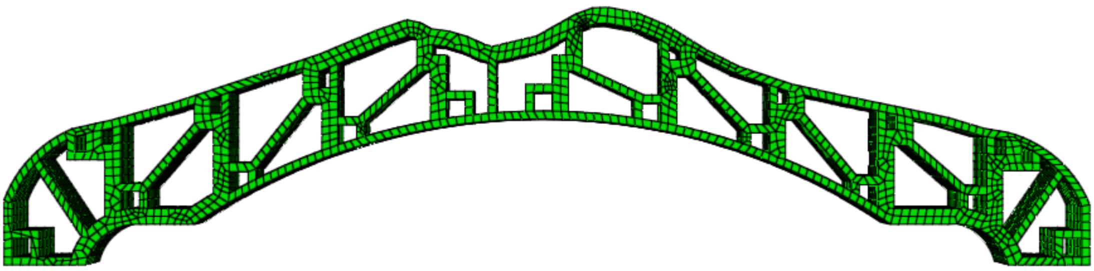

Figure 4.14 Configuration 2, numerical model

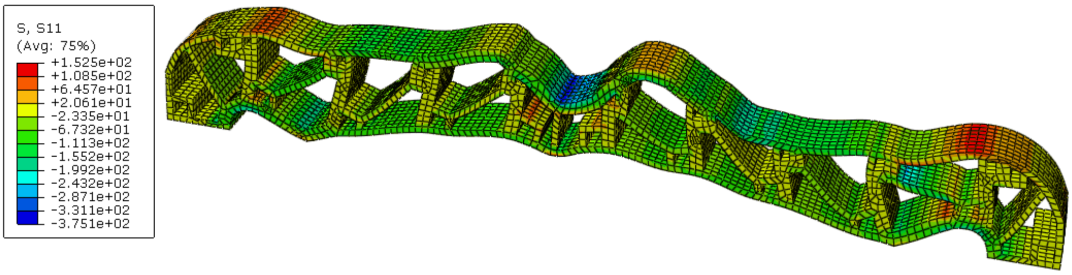

Figure 4.15 Configuration 2, concrete stress S11

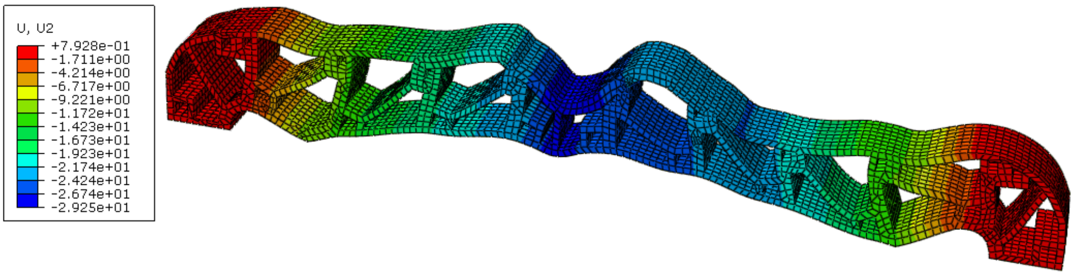

Figure 4.16 Configuration 2, displacement U2

ANALYSIS 3

Configuration 3

Boundary conditions: zipper-zipper

Load applied: gravity + concentrated forces on top side of the beam

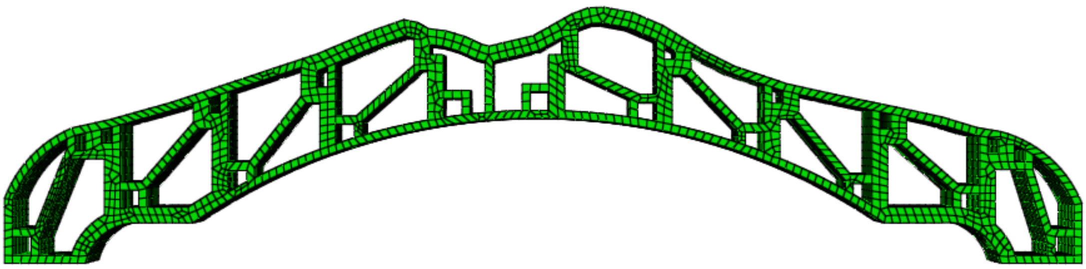

Figure 4.17 Configuration 3, numerical model

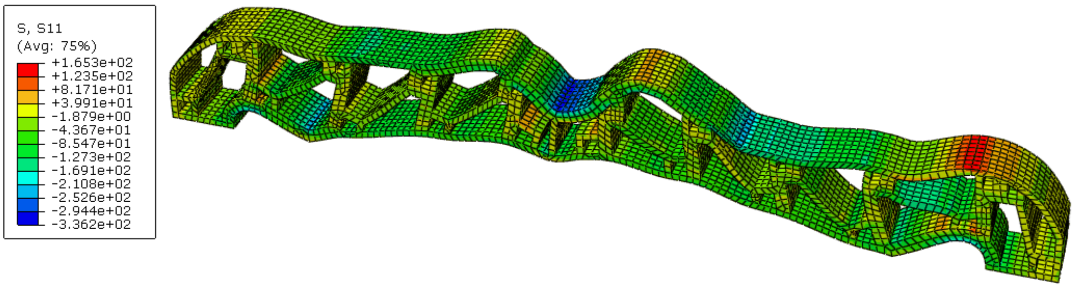

Figure 4.18 Configuration 3, concrete stress S11

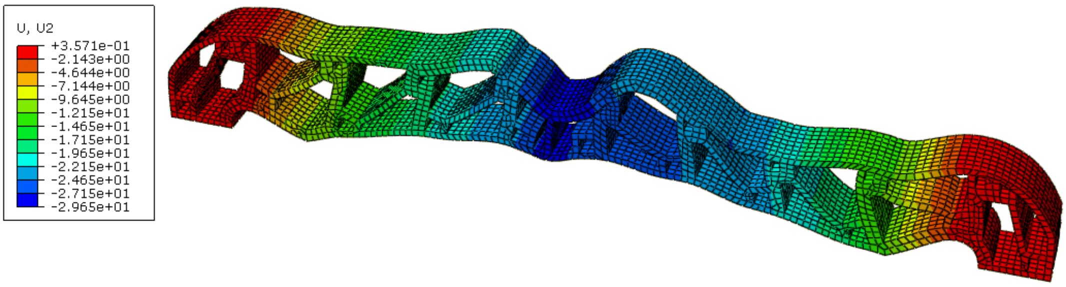

Figure 4.19 Configuration 3, displacement U2

In the tables the mid-span deflection (U2) and the maximum stress (S11) in the concrete are reported:

Configuration	Deflection(mm)	S11(N/mmq)
1	-30,7	147,1
2	-29,3	152,5
3	-29,7	165,3

Table 4.1 Results about preliminary tests

As it can be seen in the table the results magnitude exceed the standard values of the material. This phenomenon is caused by the absence of steel reinforcement bars in the models used in these tests. The analyses only aimed at verifying the correctness of the numerical model and absence of modelling defects.

4.4 *Curved beam, linear analyses*

In this section are described some of the most significant linear analyses carried out on the final beam geometry before the printing process. In these analyses it was used the aforementioned improved model.

ANALYSIS 1

Thickness configuration: 1

Boundary conditions: zipper-support + BC1

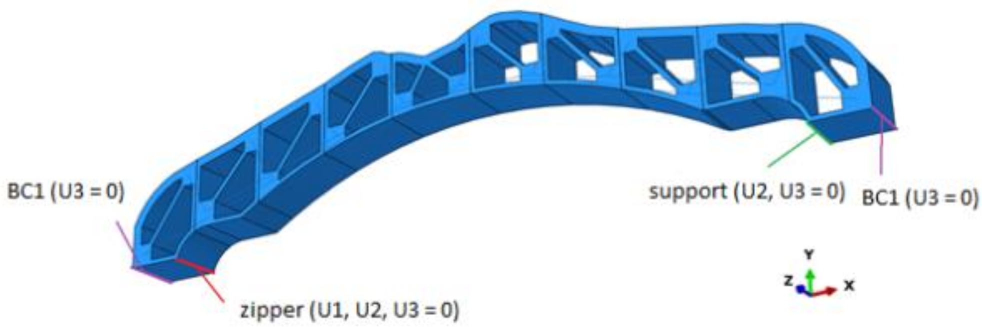

Figure 4.20 Boundary conditions 1

Constraint between concrete elements: tie on the whole contact surface

Load applied: gravity

Figure 4.21 Analysis 1, displacement U2

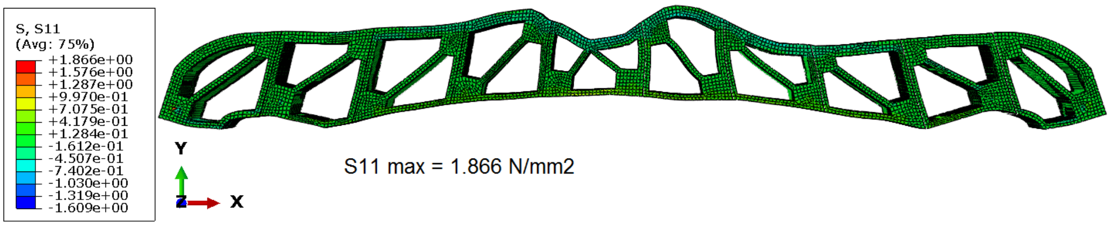

Figure 4.22 Analysis 1, concrete stress S11

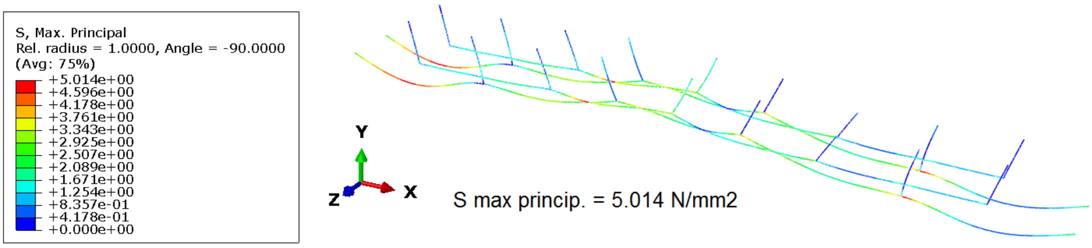

Figure 4.23 Analysis 1, max principal stress, bars

ANALYSIS 2

Thickness configuration: 1

Boundary conditions: zipper-support

Constraint between concrete elements: only CONTACT (Penalty for the Tangential Behavior; Hard Contact for the Normal Behavior).

Load applied: gravity

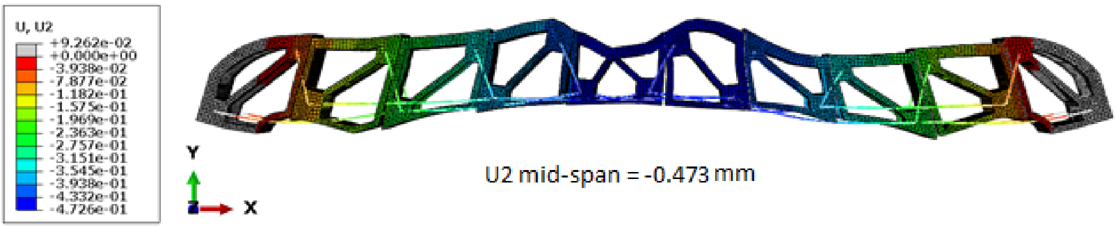

Figure 4.24 Analysis 2, displacement U2

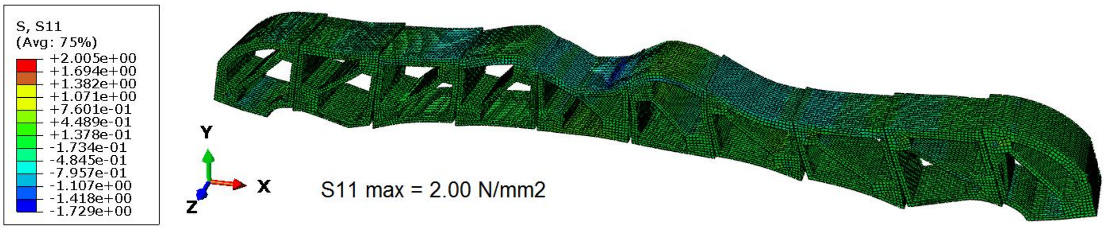

Figure 4.25 Analysis 2, concrete stress S11

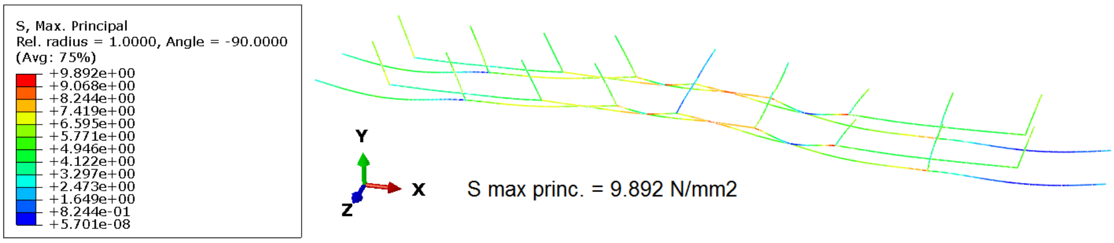

Figure 4.26 Analysis 2, max principal stress, bars

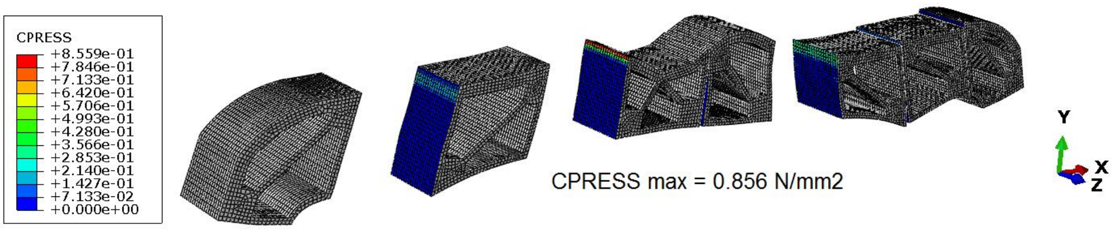

Figure 4.27 Analysis 2, contact pressure

ANALYSIS 3

Boundary conditions: zipper-zipper

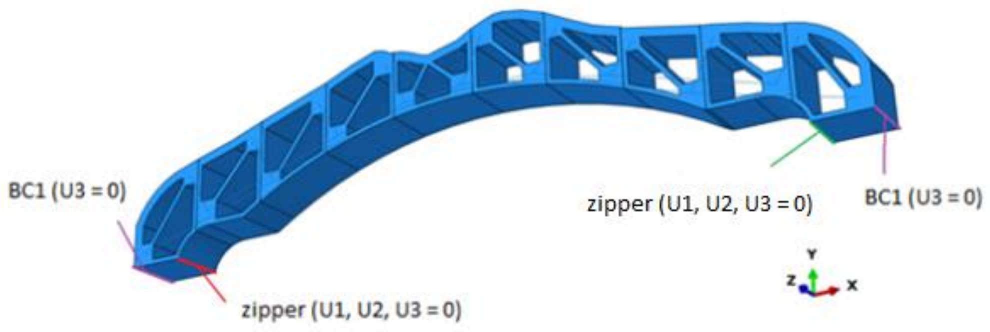

Figure 4.28 Boundary conditions 2

Thickness configuration: 1

Constraint between concrete elements: only CONTACT (Penalty for the Tangential Behavior; Hard Contact for the Normal Behavior).

Load applied: gravity

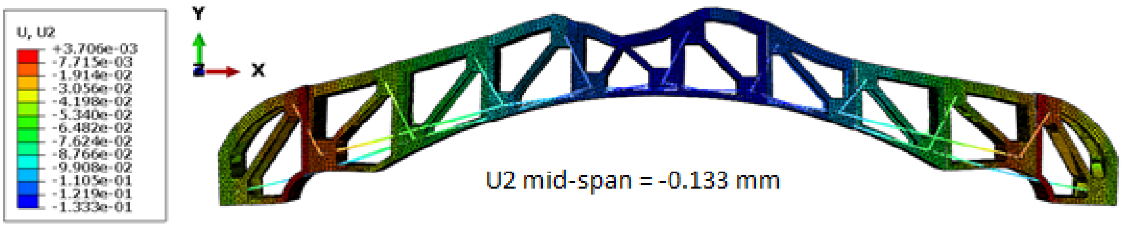

Figure 4.29 Analysis 3, displacement U2

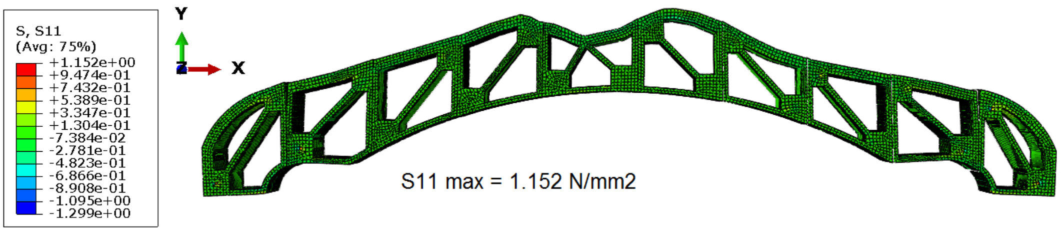

Figure 4.30 Analysis 3, concrete stress S11

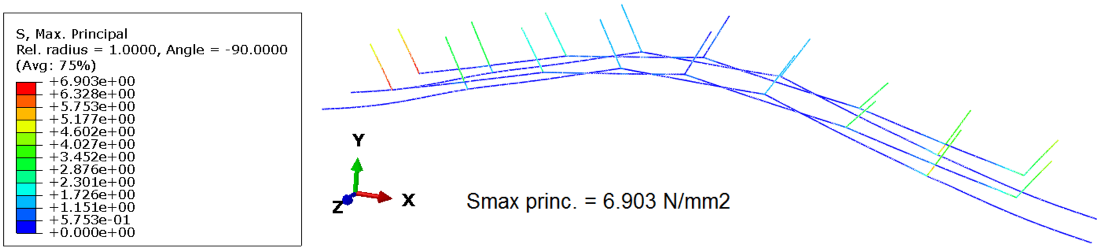

Figure 4.31 Analysis 3, max principal stress, bars

ANALYSIS 4

Boundary conditions: zipper-support

Thickness configuration: 2

Constraint between concrete elements: tie on the whole contact surface

Load applied: gravity

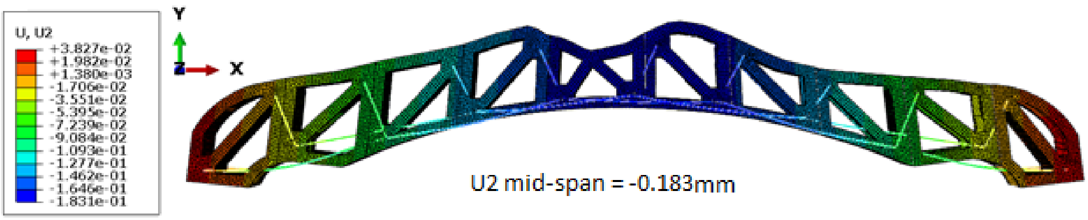

Figure 4.32 Analysis 4, displacement U2

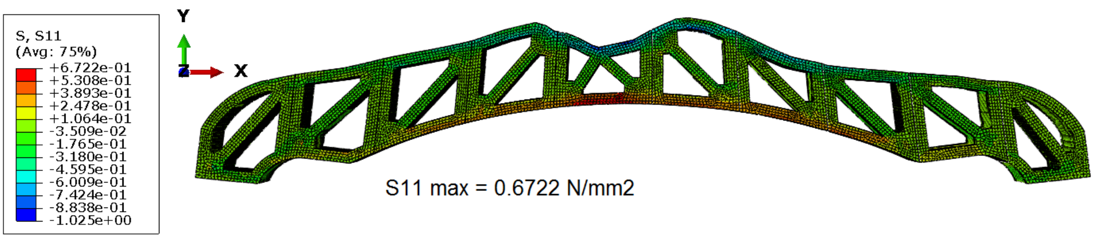

Figure 4.33 Analysis 4, concrete stress S11

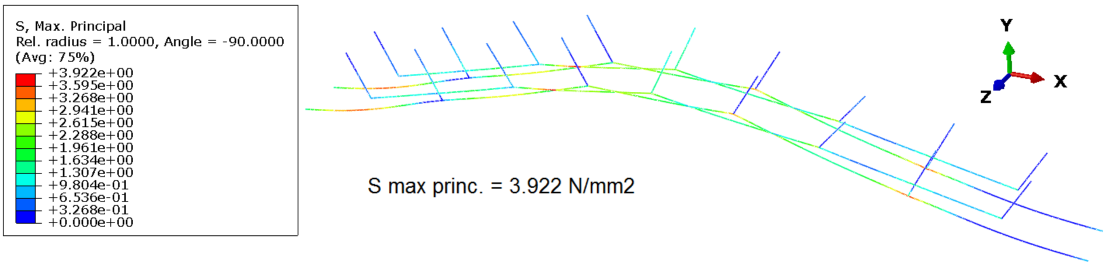

Figure 4.34 Analysis 4, max principal stress, bars

ANALYSIS 5

Boundary conditions: zipper-support

Thickness configuration: 2

Constraint between concrete elements: only CONTACT (Penalty for the Tangential Behavior; Hard Contact for the Normal Behavior).

Load applied: gravity

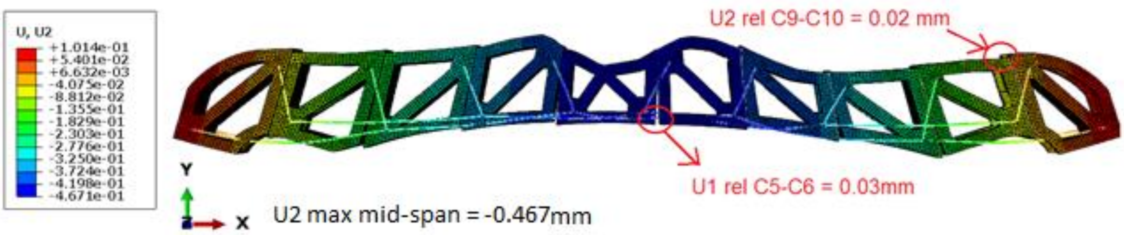

Figure 4.35 Analysis 5, displacement U2

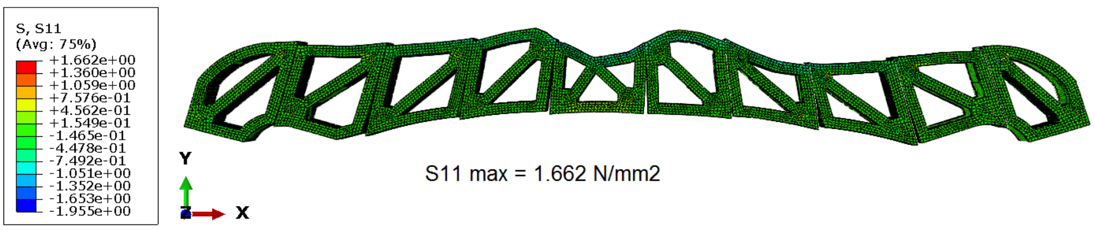

Figure 4.36 Analysis 5, concrete stress S11

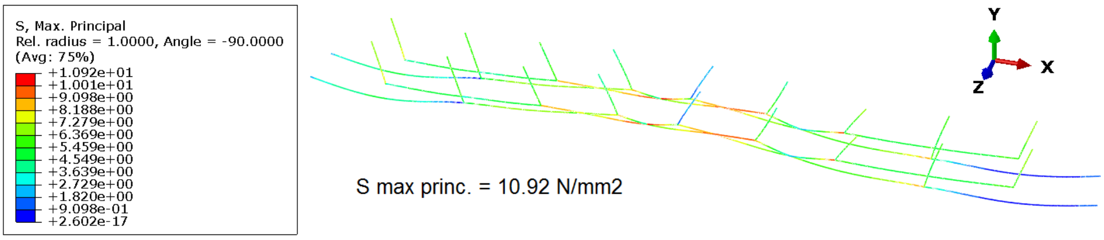

Figure 4.37 Analysis 5, max principal stress, bars

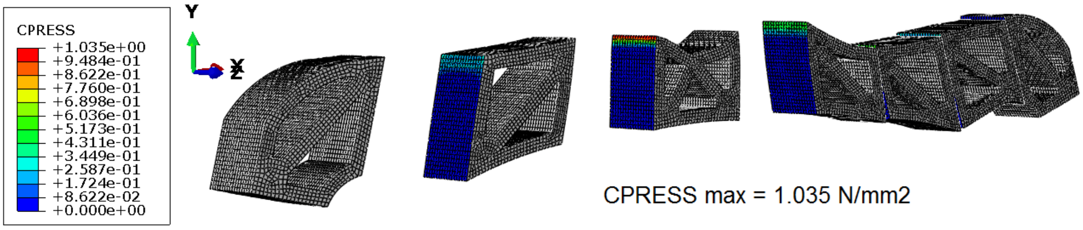

Figure 4.38 Analysis 5, contact pressure

ANALYSIS 6

Boundary conditions: zipper-zipper

Thickness configuration: 2

Constraint between concrete elements: only CONTACT (Penalty for the Tangential Behavior; Hard Contact for the Normal Behavior).

Load applied: gravity

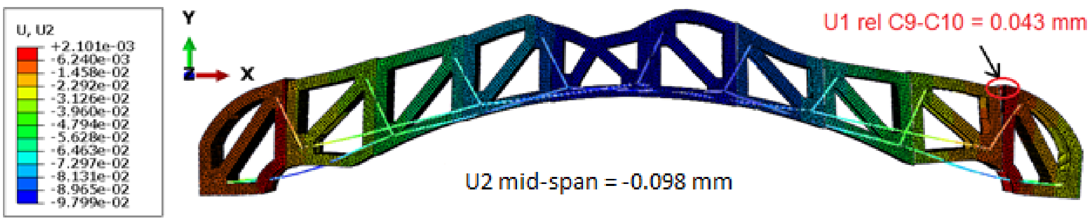

Figure 4.39 Analysis 6, displacement U2

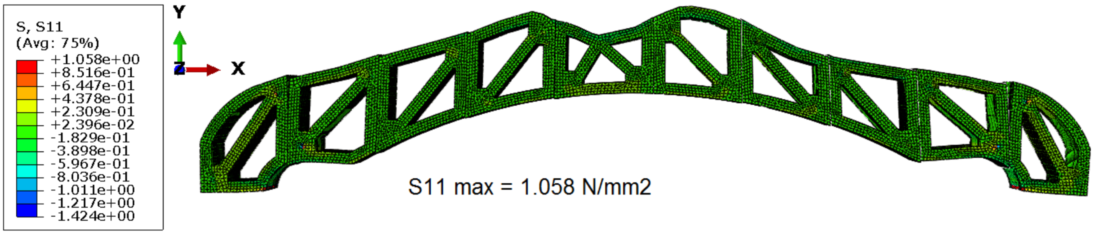

Figure 4.40 Analysis 6, concrete stress S11

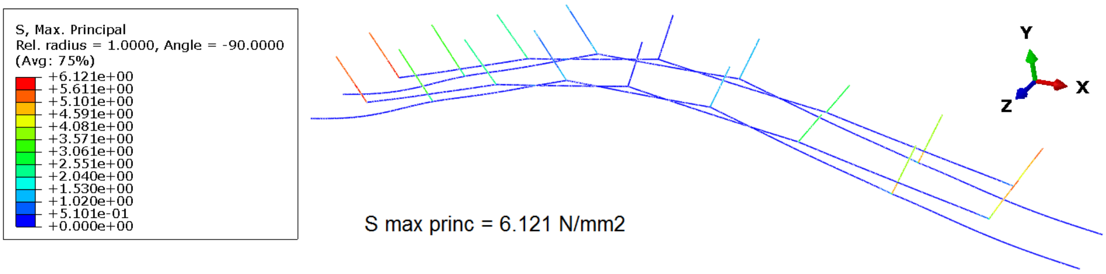

Figure 4.41 Analysis 6, max principal stress, bars

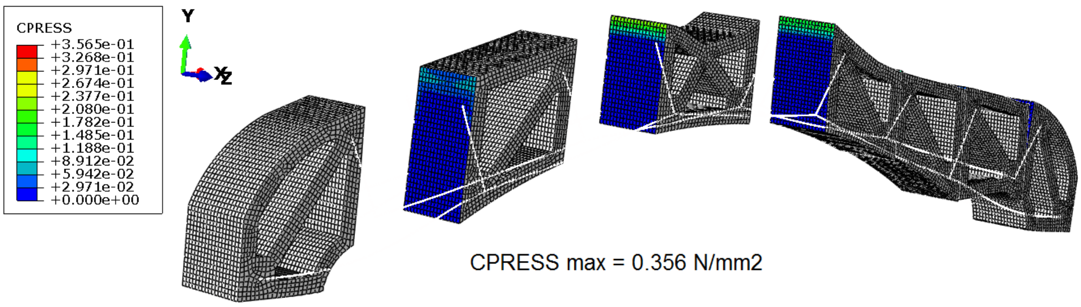

Figure 4.42 Analysis 6, contact pressure

Subsequently, to obtain a comparison in terms of results, other analyses have been made on Sap2000 software.

For these analyses the default material characteristics of Sap have been used.

ANALYSIS 7

Boundary conditions: zipper-support

Thickness configuration: 1

Constraint between concrete elements: rigid links with a release in the extremal point, on the compression zones

Load applied: gravity

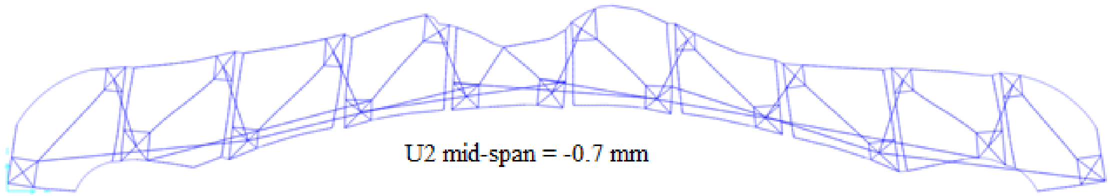

Figure 4.43 Analysis 7, displacement u2

TABLE: Joint Reactions								
Joint	OutputCase	CaseType	Forizz	Fvert	F3	M1	M2	M3
Text	Text	Text	N	N	N	N-mm	N-mm	N-mm
1	DEAD	LinStatic	0	0	34,41	360,42	-207,28	0
20	DEAD	LinStatic	-4,271E-08	2951,28	16,21	2,24	402,89	0
23	DEAD	LinStatic	0	0	40,19	207,28	-196,27	0
174	DEAD	LinStatic	0	0	40,14	358,57	181,09	0
176	DEAD	LinStatic	0	2935,68	16,82	2,18	-436,6	0
199	DEAD	LinStatic	0	0	39,93	205,42	256,19	0
			-4,271E-08	5886,96			0	

Table 4.2 Analysis 7, joint reactions

STRESS

Maximum tensile σ of concrete : 3,66 N/mm² (element 105)

Maximum σ of steel : 10,17 N/mm² (element 380)

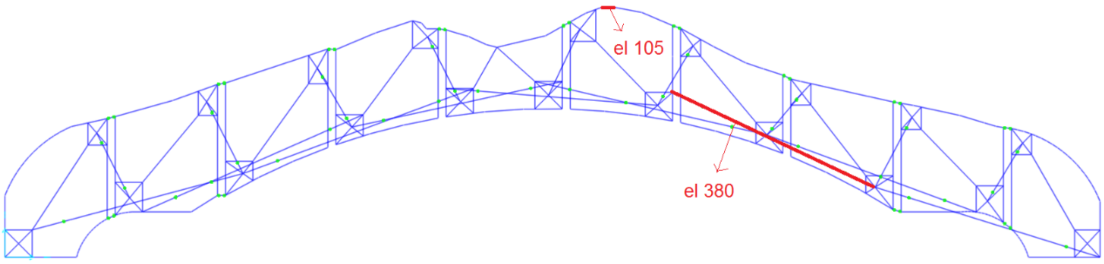

Figure 4.44 Analysis 7, most urged elements

ANALYSIS 8

Boundary conditions: zipper-support

Thickness configuration: 2

Constraint between concrete elements: rigid links with a release in the extremal point, on the compression zones

Load applied: gravity

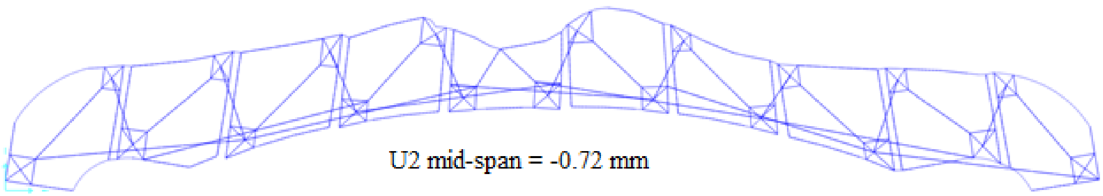

Figure 4.45 Analysis 8, displacement u2

TABLE: Joint Reactions								
Joint	**OutputCase**	**CaseType**	**Forizz**	**Fvert**	**F3**	**M1**	**M2**	**M3**
Text	Text	Text	N	N	N	N-mm	N-mm	N-mm
1	DEAD	LinStatic	0	0	36,41	300,35	-300,35	0
20	DEAD	LinStatic	1,061E-08	3382,88	27,02	3,74	671,49	0
23	DEAD	LinStatic	0	0	53,78	172,74	-372,23	0
174	DEAD	LinStatic	0	0	41,75	298,8	261,3	0
176	DEAD	LinStatic	0	3318,78	28,03	3,63	-727,67	0
199	DEAD	LinStatic	0	0	53,54	171,19	467,51	0
			1,061E-08	6701,66			0	

Table 4.3 Analysis 8, joint reactions

STRESS

Maximum tensile σ of concrete : 1,33 N/mm² (element 80)

Maximum σ of steel : 11,34 N/mm² (element 379-380)

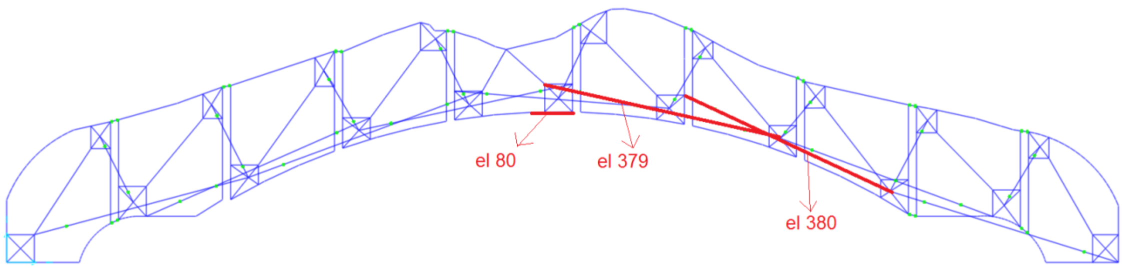

Figure 4.46 Analysis 8, most urged elements

This summary table shows the most significant results of linear analyses:

ANALYSIS	THICKNESS CONFIGURATION	BOUNDARY CONDITIONS	LOAD APPLIED	CONSTRAINT/ INTERACTION	U2 MAX MID-SPAN (mm)	S11 MAX CONCRETE (Mpa)	S MAX PRINCIPAL, BARS (Mpa)	CONTACT PRESSURE MAX (Mpa)
1	1	zipper-support	gravity	tie	-0,211	1,866	5,014	-
2	1	zipper-support	gravity	contact	-0,473	2	9,892	0,856
3	1	zipper-zipper	gravity	contact	-0,133	1,152	6,903	-
4	2	zipper-support	gravity	tie	-0,183	0,6722	3,922	-
5	2	zipper-support	gravity	contact	-0,467	1,662	10,92	1,035
6	2	zipper-zipper	gravity	contact	-0,098	1,058	6,121	0,356
7	1	zipper-support	gravity	rigid links	-0,7	3,66	10,17	-
8	2	zipper-support	gravity	rigid links	-0,72	1,33	11,34	-

Table 4.4 Summary table of results of linear analyses

4.5 Curved beam, non-linear analyses

In this paragraph the most significant non-linear analyses are reported with a schematic description of their characteristic.

In order to facilitate reading the analyses reported, following, an explanatory scheme shows the structure of this paragraph:

- the first subsection reports the first range of analyses that encompasses the four base model used to implement all other ones;
- the second one reports the most important analyses in terms of stresses, strains and displacement applied.

Furthermore, in the end of each subsection, a summary table of results is reported.

Finally in the end of chapter, in the above mentioned tables, also we will report the results of some analyses that will not be shown in the following pages, relevant for the comparisons which will be made in the next chapter to draw some conclusions.

4.5.1 Non-linear analyses on final geometry configuration

In this subsection the first analyses group on the four base models will be reported. It must be remembered that in this analyses only the material parameters has been changed in order to obtain a direct comparison with the linear ones.

MODEL 1

Boundary conditions: zipper-support

Thickness configuration: 1

Constraint between concrete elements: tie on the whole contact surface

Load applied: gravity

Figure 4.47 Base model 1, displacement U2

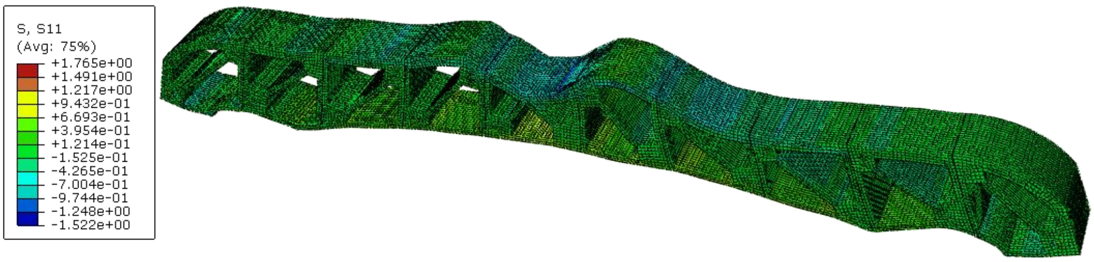

Figure 4.48 Base model 1, concrete stress S11

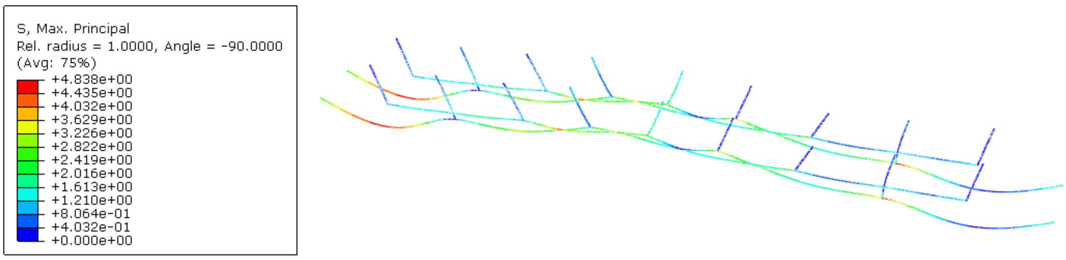

Figure 4.49 Base model 1, max principal stress, bars

MODEL 2

Boundary conditions: zipper-support

Thickness configuration: 1

Constraint between concrete elements: only CONTACT (Penalty for the Tangential Behavior; Hard Contact for the Normal Behavior).

Load applied: gravity

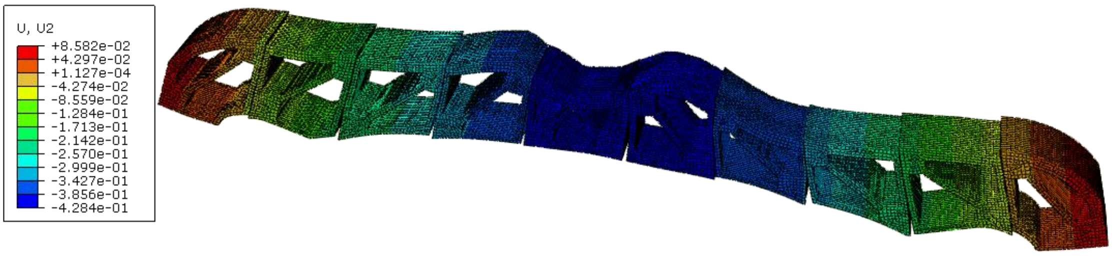

Figure 4.50 Base model 2, displacement U2

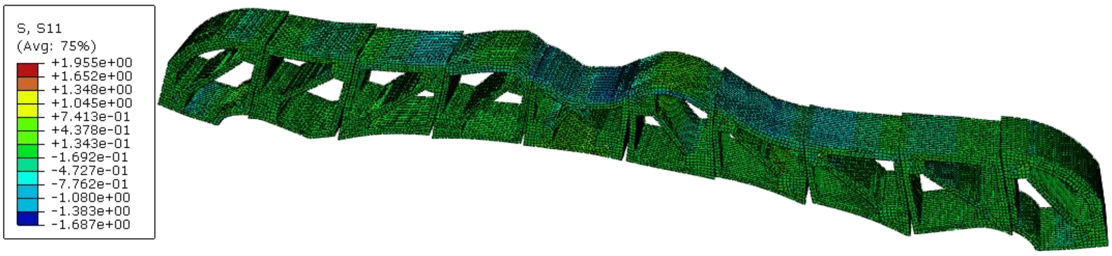

Figure 4.51 Base model 2, concrete stress S11

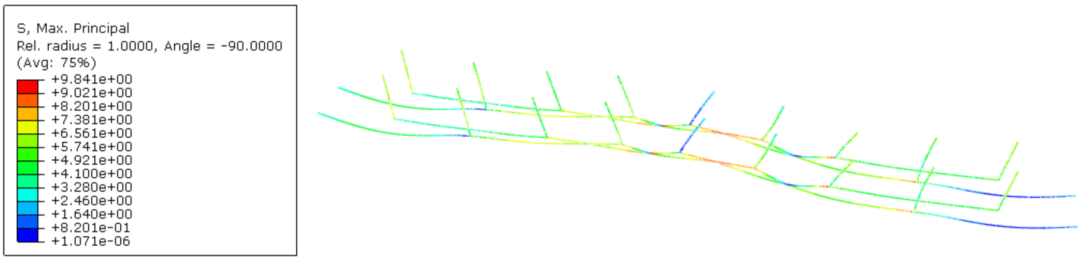

Figure 4.52 Base model 2, max principal stress, bars

MODEL 3

Boundary conditions: zipper-support

Thickness configuration: 2

Constraint between concrete elements: tie on the whole contact surface

Load applied: gravity

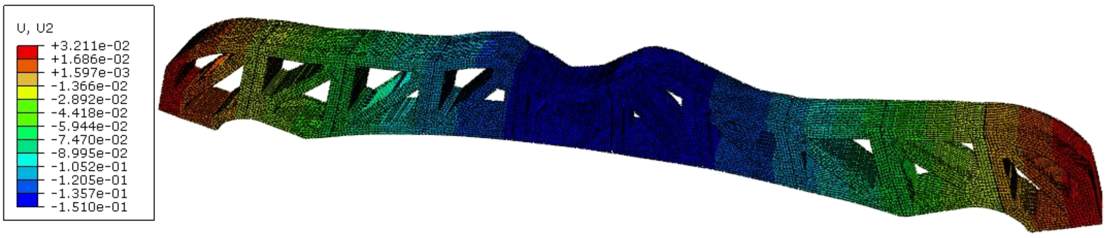

Figure 4.53 Base model 3, displacement U2

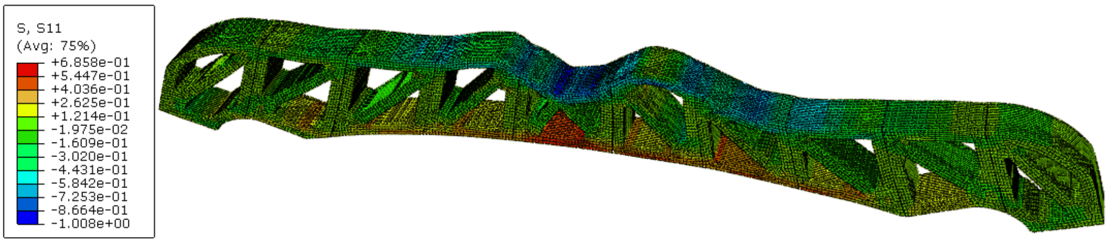

Figure 4.54 Base model 3, concrete stress S11

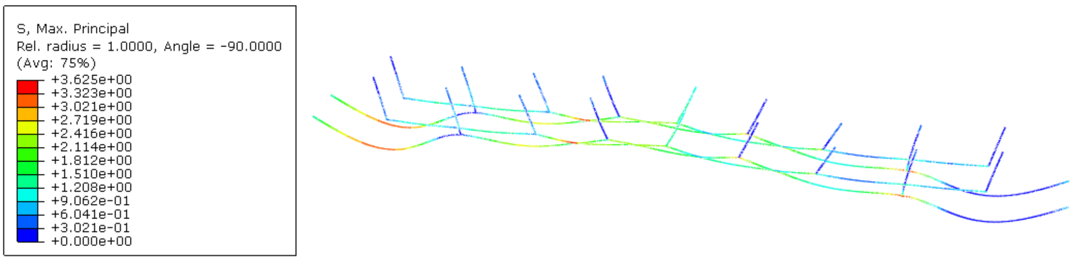

Figure 4.55 Base model 3, max principal stress, bars

MODEL 4

Boundary conditions: zipper-support

Thickness configuration: 2

Constraint between concrete elements: only CONTACT (Penalty for the Tangential Behavior; Hard Contact for the Normal Behavior).

Load applied: gravity

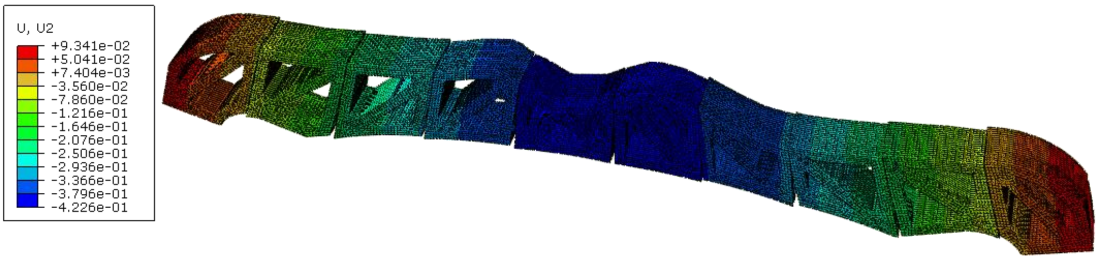

Figure 4.56 Base model 4, displacement U2

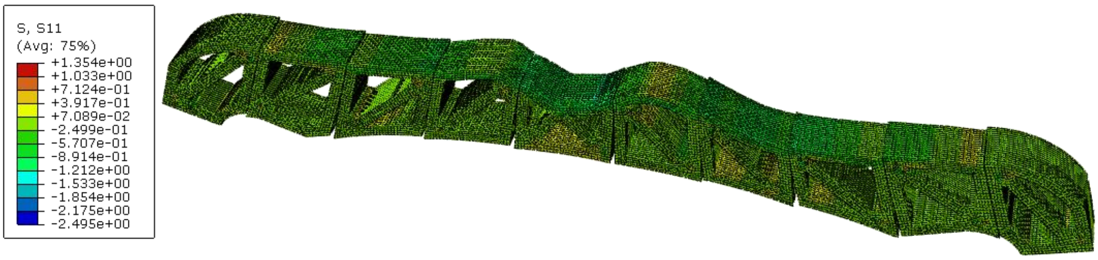

Figure 4.57 Base model 4, concrete stress S11

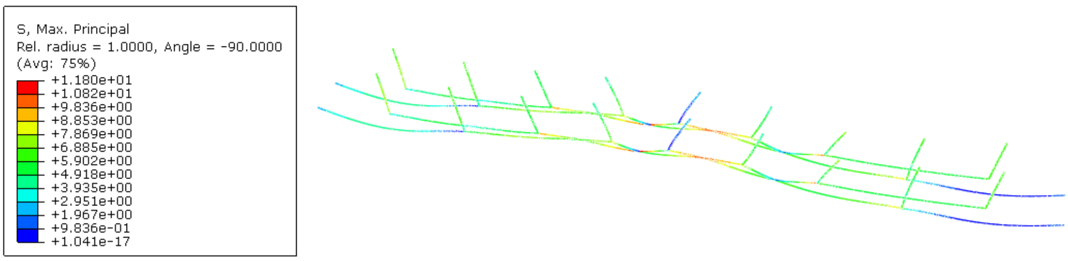

Figure 4.58 Base model 4, max principal stress, bars

MODEL		BOUNDARY CONDITIONS	THICK. CONF.	U2 MAX MID-SPAN (mm)	U2 MAX SUPPORT (mm)	U1 MAX SUPPORT (mm)	S MAX PRINCIPAL STEEL BARS (Mpa)	S11(-) CONCRETE (Mpa)	S11(+) CONCRETE (Mpa)	TIME
1	tie	zipper-support	1	-0,03181	0,1749	0,1822	4,84	-1,522	1,765	1'
2	contact	zipper-support	1	-0,428	0,0858	0,4321	9,841	-1,687	1,955	14'
3	tie	zipper-support	2	-0,151	0,0321	0,149	3,625	-1,01	0,686	58''
4	contact	zipper-support	2	-0,423	0,0934	0,434	11,8	-2,495	1,354	27'

Table 4.5 Summary table of results of base models

4.5.2 *Most relevant analyses*

This subsection provides an overview in the most urged models. To avoid confusion, starting from this point, the analyses will be named with the acronym DCA”x” (Displacement Controlled Analysis) in which “x” is the progressive number.

Whereas the steel bars always remain in the elastic behavior, in the following figures, only the screenshot about concrete stresses will be reported for each case.

DCA 1

Boundary conditions: zipper-support

Thickness configuration: 1

Constraint between concrete elements: tie on the whole contact surface

Load applied: gravity

Displacement entity: 2 mm

Displacement application: on the mid-span section set

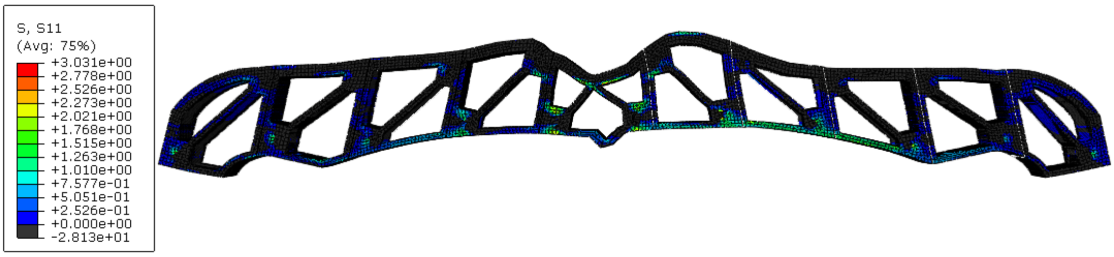

Figure 4.59 DCA 1, concrete stress S11

DCA 2

Boundary conditions: zipper-support

Thickness configuration: 1

Constraint between concrete elements: tie on the whole contact surface

Load applied: gravity

Displacement entity: 2 mm

Displacement application: on a reference point in the mid-span section

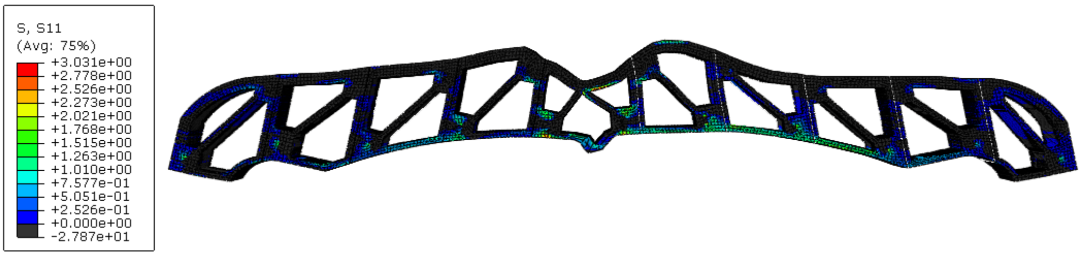

Figure 4.60 DCA 2, concrete stress S11

DCA 3

Boundary conditions: zipper-support

Thickness configuration: 1

Constraint between concrete elements: tie on the whole contact surface

Load applied: gravity

Displacement entity: 3 mm

Displacement application: on a reference point in the mid-span section

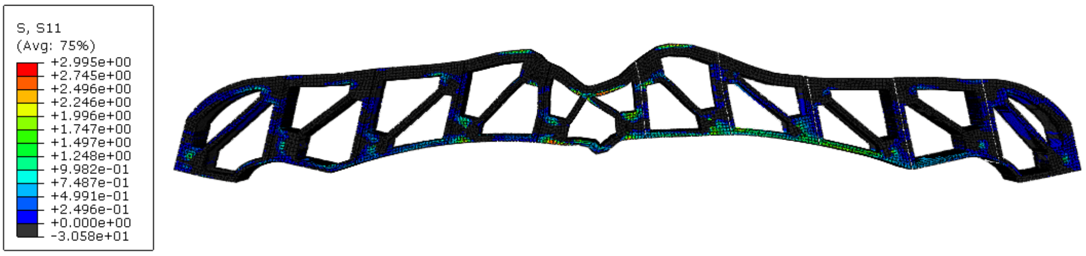

Figure 4.61 DCA 3, concrete stress S11

DCA 4

Boundary conditions: zipper-support

Thickness configuration: 1

Constraint between concrete elements: only CONTACT (Penalty for the Tangential Behavior; Hard Contact for the Normal Behavior).

Load applied: gravity

Displacement entity: 2 mm

Displacement application: on a reference point in the mid-span section

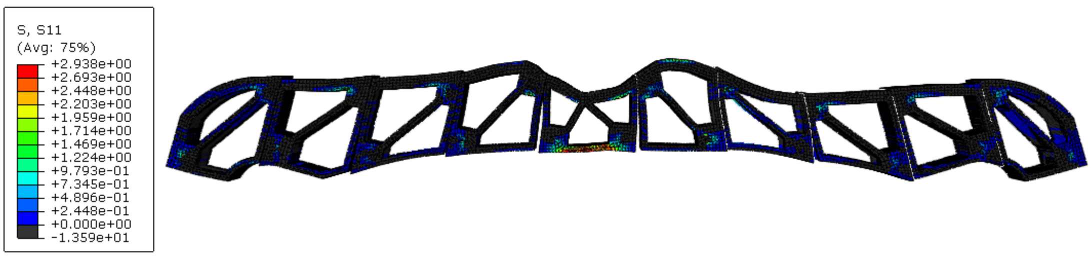

Figure 4.62 DCA 4, concrete stress S11

DCA 5

Boundary conditions: zipper-support

Thickness configuration: 2

Constraint between concrete elements: tie on the whole contact surface

Load applied: gravity

Displacement entity: 2 mm

Displacement application: on a reference point in the mid-span section

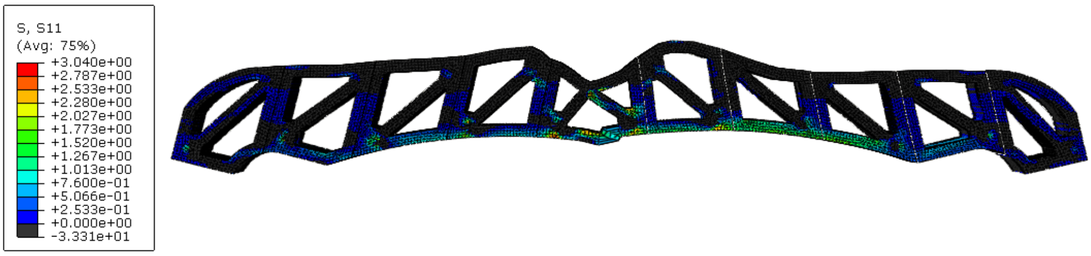

Figure 4.63 DCA 5, concrete stress S11

DCA 6

Boundary conditions: zipper-support

Thickness configuration: 2

Constraint between concrete elements: only CONTACT (Penalty for the Tangential Behavior; Hard Contact for the Normal Behavior).

Load applied: gravity

Displacement entity: 2 mm

Displacement application: on the mid-span section set

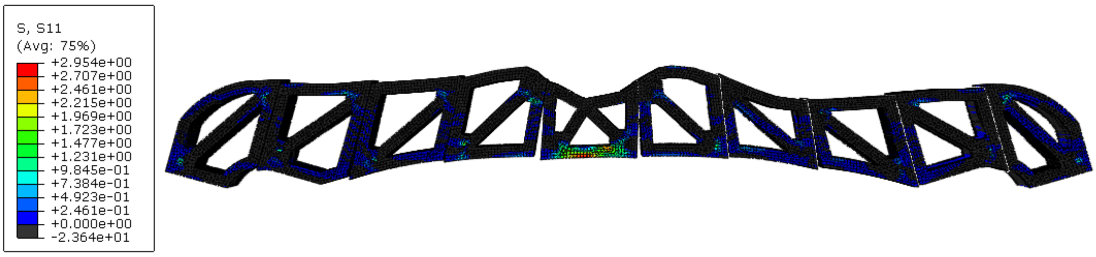

Figure 4.64 DCA 6, concrete stress S11

DCA 7

Boundary conditions: zipper-support

Thickness configuration: 2

Constraint between concrete elements: only CONTACT (Penalty for the Tangential Behavior; Hard Contact for the Normal Behavior).

Load applied: gravity

Displacement entity: 2 mm

Displacement application: on a reference point in the mid-span section

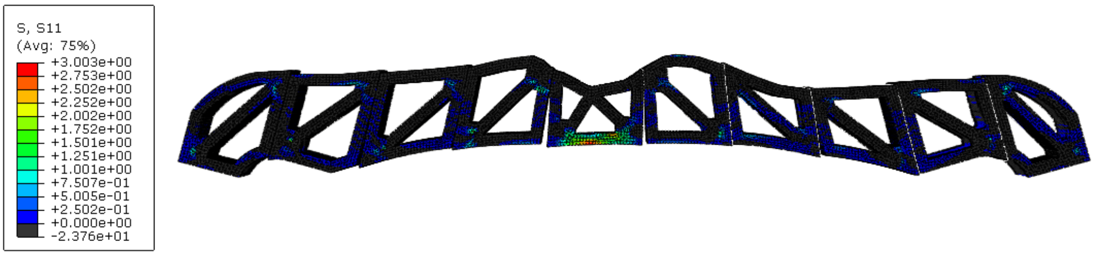

Figure 4.65 DCA 7, concrete stress S11

DCA 8

Boundary conditions: zipper-support

Thickness configuration: 2

Constraint between concrete elements: only CONTACT (Penalty for the Tangential Behavior; Hard Contact for the Normal Behavior).

Load applied: gravity

Displacement entity: 3 mm

Displacement application: on the mid-span section set

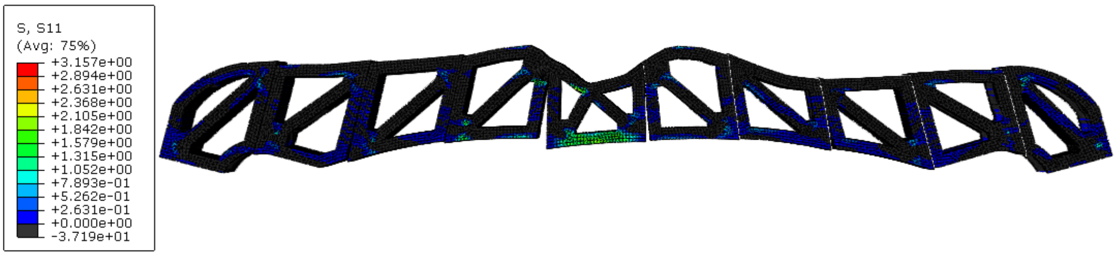

Figure 4.66 DCA 8, concrete stress S11

CDA	INTERACTION	DISPLACEMENT CONFIGURATION	U2 MAX MID-SPAN (mm)	U2 MAX SUPPORT (mm)	U1 MAX SUPPORT (mm)	S MAX PRINCIPA L STEEL BARS (Mpa)	S11(-) CONCRETE (Mpa)	S11(+) CONCRETE (Mpa)	TIME
1	Tie	2 mm on the mid-span section set	-2,309	0,35	1,873	95,45	-28,13	3,031	1 : 24'
2	Tie	2 mm on a reference point in the mid-span section	-2,393	0,3489	1,878	95,04	-27,87	3,031	1 : 32'
3	Tie	3 mm on a reference point in the mid-span section	-3,376	0,509	2,732	110,6	-30,58	2,995	2:3'
4	Contact	2 mm on the reference point in the mid-span section	-2,041	0,4007	2,026	55,46	-13,39	2,938	40'
5	Tie	2mm on a reference point in the mid-span section	-2,14	0,385	1,858	87,79	-33,31	3,04	4:33'
6	Contact	2 mm on the mid-span section set	-2,034	0,427	2,055	64,47	-23,64	2,954	1:9'
7	Contact	2mm on a reference point in the mid-span section	-2,034	0,427	2,056	64,55	-23,76	3,003	1:5'
8	Contact	3 mm on the mid-span section set	-3,01	0,599	2,86	92,65	-37,19	3,157	15:43'

Table 4.6 Summary table of results of CDA

Finally, in the next table are reported all the results about the analyses that hasn’t been shown.

ANALYSIS	INTERACTION/ THICK. CONF.	DISPLACEMENT CONFIGURATION	U2 MAX MID-SPAN (mm)	U2 MAX SUPPORT (mm)	U1 MAX SUPPORT (mm)	S MAX PRINCIPAL STEEL BARS (Mpa)	S11(-) CONCRETE (Mpa)	S11(+) CONCRETE (Mpa)	TIME
1	Tie/1	1 mm on the mid-span section set	-1,226	0,1765	0,9694	54,49	-13,35	2,92	52'
2	Tie/1	1 mm horizontal on the right support	-0,97	0,1769	1	35,85	-20,59	2,563	32'
3	Tie/1	1mm on a reference point in the mid-span section	-1,19	0,1776	0,9709	52,73	-12,29	2,89	37'
4	Tie/1	2 mm horizontal on the right support	ABORTED						
5	Contact/1	1 mm on the mid-span section set	-1,027	0,2036	1,025	26,81	-6,953	2,27	17'
6	Contact/1	1mm on a reference point in the mid-span section	-1,025	0,2036	1,025	26,89	-6,561	2,394	17'
7	Contact/1	2 mm on the mid-span section set	ABORTED						
8	Contact/1	3 mm on the reference point in the mid-span section	ABORTED						
9	Tie/2	2 mm on the mid-span section set	ABORTED						
10	Contact/2	3 mm on the mid-span section set	ABORTED						
11	Contact/2	3mm on the reference point in the mid-span section	ABORTED						
12	Contact/2	3mm on the reference point in the mid-span section	ABORTED						

Table 4.7 Summary table of results of not mentioned analyses

5 Conclusions and future developments

5.1 Considerations about numerical modelling

Comparing the results of linear analyses number 1, 2, 4, 5 reported in table 4.4 (page 84) and the results of non-linear ones reported in table 4.5 (page 90), it can be seen that, under the self-weight of the beam, the order of magnitude of the results is compatible:

	NON-LINEAR ANALYSES ON FINAL GEOMETRY CONFIGURATION				LINEAR ANALYSES ON FINAL GEOMETRY CONFIGURATION			
	1	2	3	4	1	2	4	5
U2 MAX MID-SPAN (mm)	-0,03181	-0,428	-0,151	-0,423	-0,211	-0,473	-0,183	-0,467
S11(+) CONCRETE (Mpa)	1,765	1,955	0,686	1,354	1,866	2	0,6722	1,662

Table 5.1 Comparison between results of non-linear analyses on final geometry configuration and the linear ones.

This allows us to observe that the non-linear material implemented does not alter the elastic behavior. The mid-span deflection and the concrete stresses are in the right range if we consider that the characteristic tensile resistance of the concrete is about 2.975 MPa.

Another important aspect will be analyzed: the duration of the analyses and the convergence difficulty of the solving algorithm. Through observation of the data concerning the duration of each analysis in tables 4.5, 4.6, 4.7 it can be noted that, according to the models taken into exam and the magnitude of the imposed displacement, the duration of the analyses varies from a few minutes to many hours and in some cases it failed. In detail, in the fourteen analyses with configuration of thickness number 1, only three failed (two with Contact interaction) while in the ten analyses with the configuration of thickness number 2, only three failed (three with Tie constraint) overturning the trend.

The convergence difficulty of the analyses is related to the complex geometry of the beam, the local distortion, caused by the imposed displacement, and the size of the mesh elements.

5.2 *Considerations about steel and concrete behavior*

Observing the controlled displacement analyses (DCA) shown in the previous chapter, it can be noted that the tensile stresses of concrete are very close to the threshold value in some cases, but in most ones they exceeded it making such values (3 MPa) not acceptable. Regarding the steel reinforcement bars, it can be seen that they are not over 391 MPa which is the elastic limit. The following table indicates the results highlighted in green color in tables 4.4, 4.6, showing the difference between the tensile stresses between the linear analyses and the controlled displacements ones:

	LINEAR ANALYSES							
	1	2	3	4	5	6	7	8
S11(+) CONCRETE (Mpa)	1,866	2	1,152	0,6722	1,662	1,058	3,66	1,33
	CDA							
	1	2	3	4	5	6	7	8
S11(+) CONCRETE (Mpa)	3,031	3,031	2,995	2,938	3,04	2,954	3,003	3,157

Table 5.2 Comparison between tensile stresses

The two materials have different behavior because perfect adherence between them is lacking and therefore the stresses transmission is inadequate, leading the concrete to a fragile breaking, while the steel bars are not yielded.

Among the figures showing the stresses trend in the concrete elements, it can be noted that:

- in the models with the Tie constraint, the tensile stresses are more spread while,

- in the models with a Contact interaction the tensile stresses concentrated on the intrados of the central block.

Moreover, in the models with the Tie constraint and configuration of thickness number 1, it can be seen a located distortion in the section where the displacement is applied (amplified by scale effect), while in the same models with Contact interaction and configuration of thickness number 2 it cannot be observed.

5.3 Future developments

The possible future development regarding these studies about the structural behavior of a 3D-printed beam can be aimed at improving some aspects, in order to obtain satisfactory results characterizing this technology.

The first point on which it is needed to work, is linked to the magnitude of the tensile stresses in concrete, in order to make them not to exceed the standard values. On this point, new assembly technologies between the blocks could be elaborated and it could be tried to re-establish the perfect adherence between the outer rebar system and the concrete. It is a fundamental aspect for the behavior of reinforced concrete beams, made with a traditional techniques.

In this context, some optimization algorithms described in chapter 2 could be used, but they are not used in this analysis phase yet. It is possible to modify the shape of the blocks with the help of such algorithms and to guarantee, at the same time, the maximum material removal, preserving the resistance and stiffness characteristics of the beam.

In addition, to improve the analyses quality, it could be needed to reduce further the size of the mesh elements, even if this increases the burdensomeness of the same in time and data volume terms.

It is advisable to focus on the models where Tie constraint was used, as it mirrors greatly the final condition of the printed beam. This is assembled interposing a special mortar among the concrete blocks, giving a good monolithicity level.

Bibliography

[1] Roberto Naboni, Ingrid Paoletti (2015). Advanced Customization in Architectural Design and Construction. Springer, Milan.

[2] Ottimizzazione Strutturale (2015). https://cdm.ing.unimo.it/files/.

[3] J. Gordon. Structures or Why Things Don't Fall Down (1978). Penguin, Baltimore.

[4] P.W. Christensen, A. Klarbring (2009). An Introduction to Structural Optimization. Springer, Waterloo, Ontario, Canada.

[5] Ottimizzazione Strutturale: ottimizzazione parametrica, topologica, di forma. http://www.smartcae.com/applicazioni/ottimizzazione-strutturale/.

[6] http://www.costruirecorrettamente.org.

[7] Dr. I. Gibson, Dr. D.W. Rosen, Dr. B. Stucker (2015). Additive Manufacturing Technologies: 3D printing, Rapid Prototyping to Direct Digital Manufacturing. Springer, New York.

[8] J.B. Mander, M.J.N. Priestley, R. Park, Fellow, ASCE (1988). Theoretical stress-strain model for confined concrete, taken from *Journal of Structural Engineering*,Vol. 114, No. 8.

[9] Introduction to Finite Elements Abaqus Handout and Nuclear Engineering Table of Contents. http:/www.academia.edu.

[10] SIMULIA Dessault Sistémes. Abaqus 6.12. Abaqus/CAE User’s Manual.

Even if they were not mentioned directly, further references were:

[11] R.A. Buswell, R.C. Soar, A.G.F. Gibb, A. Thorpe (2006). Freeform Construction: Mega-scale Rapid Manufacturing for construction. www.elsevier.com/locate/autcon.

[12] Giovanni Cesaretti, Enrico Dini, Xavier DeKestelier, Valentina Colla, Laurent Pambaguian (2014). Building components for an outpost on the Lunar soil by means of a novel 3D printing technology. www.elsevier.com/locate/actaastro.

[13] Edward Allen, Waclaw Zalewski (2009). Form and forces, designing efficient, expressive structures. John Wiley and Sons, Inc, Hoboken, New Jersey.

[14] Peng Feng, Xinmiao Meng, Jian-Fei Chen, Lieping Ye (2015). Mechanical properties of structures 3D printed with cementitious powders. www.elsevier.com/locate/conbuildmat.

Special thanks

Feeeeermi tutti!! Dopo aver letto tutta questa roba, se l’avete letta tutta, di cui, probabilmente, non avete capito nulla, questa è l’unica pagina che vi interessa leggere!

Proprio così, perché è giunto il momento di ringraziare tutti, ma veramente tutti, quelli che mi hanno aiutato, supportato, incitato ma anche quelli che mi hanno fatto arrabbiare, quelli che non voglio più vedere e quelli di cui, per fortuna, mi dimenticherò.

Dunque il mio primo grande ringraziamento va a tutta la mia famiglia, che non ha mai smesso di credere in me e mi ha aiutato e supportato in questo lungo e tortuoso percorso. A mia mamma, la quale il venerdì mattina mi svegliava con l’aspirapolvere nelle orecchie, sebbene ci fossero sei giorni a settimana in cui non ero a casa al mattino; a mio padre, che continuava a ripetere che ero sempre a quota esami dati uguale a zero, quando ne avevo già dati parecchi; a mia sorella che nonostante sia un continuo litigare quando serve c’è, e ai miei nonni che tengono di più alla mia istruzione che a godersi la loro pensione…a tutti voglio dare il mio sincero e profondo ringraziamento.

Un ringraziamento davvero speciale è rivolto alla mia fidanzata, Angela. Mai una parola di sconforto è uscita dalla tua bocca per me, solo sostegno e fiducia nelle mie capacità. Sono certo che senza il tuo appoggio non avrei trovato la forza di andare avanti negli ultimi mesi di questa avventura.

Ringrazio tutti i miei compagni di università perché studiare con loro è stata un’esperienza appagante. Ringrazio tutto il personale universitario, che offre la possibilità a ogni studente di svolgere questo percorso al meglio, ringrazio la segreteria e soprattutto il bar e i baristi, che avevano sempre una battuta pronta quando studiavamo fin oltre l’orario delle lezioni, Dio solo sa quante focaccine ci siamo mangiati.

Ringrazio “*il marter*” Gianluca Vigoni, con il quale ho condiviso tutti questi anni fin dal principio e con il quale, ora, ho un rapporto di amicizia che va oltre l’ambito universitario.

Ringrazio Davide “Dado” Sala, “*il grande*”, Grande, meno male che c’eri tu, con i nostri discorsi sui trattori e la campagna passavano anche le giornate più pesanti. Am racumandi eh, sempar in sima al tratur!! Vai grandeeeeeeee crr crrcr crrrrrrrrrrrr.

Voglio dare un ringraziamento particolare ai miei amici e compagni di studio, Baldini Gianluca e Crivellaro Nicolò, raga, passare le giornate in vostra compagnia e preparare gli esami insieme è stata un'esperienza che non dimenticherò.

È un dovere e un onore per me, ringraziare il mio fedele amico e compagno di studi, Francesco Martini, Fra, grazie, ho imparato tanto in questi anni da te, sei un grand'uomo e ci sei sempre stato per tutto, non ti sei mai tirato indietro quando avevo bisogno di te, studiare insieme mi ha dato una marcia in più, davvero!

Senza di voi ragazzi, non sarei neanche lontanamente riuscito a raggiungere il traguardo che ora stiamo raggiungendo insieme. Spero che il nostro rapporto di amicizia continui anche nella vita extrauniversitaria.

Grazie a tutti voi e a tutti quelli che in qualche modo hanno dato un contributo in qualsivoglia modo che mi ha aiutato in questi anni.

Infine voglio fare un forte augurio ai miei amici che devono ancora finire gli esami, ragazzi io ho finito ora tocca a voi, forza!